

AN AEROSOL - CLOUD CONDENSATION NUCLEI
AND CLOUD DROPLET CONCENTRATION CLOSURE STUDY

by

Gökhan Sever

A Thesis

Submitted to the Graduate Faculty

of the

University of North Dakota

in partial fulfillment of the requirements

for the degree of

Master of Science

Grand Forks, North Dakota

December

2010

c 2010 Gökhan Sever

This thesis, submitted by Gökhan Sever in partial fulfillment of the requirements for the degree of Master of Science from the University of North Dakota, has been read by the Faculty Advisory Committee under whom the work has been done and is hereby approved.

Chairperson

This thesis meets the standards for appearance, conforms to the style and format requirements of the Graduate School of the University of North Dakota, and is hereby approved.

Dean of the Graduate School

Date

PERMISSION

Title An Aerosol - Cloud Condensation Nuclei and Cloud Droplet
Concentration Closure Study

Department Atmospheric Sciences

Degree Master of Science

In presenting this thesis in partial fulfillment of the requirements for a graduate degree from the University of North Dakota, I agree that the library of this University shall make it freely available for inspection. I further agree that permission for extensive copying for scholarly purposes may be granted by the professor who supervised my thesis work or, in her absence, by the chairperson of the department or the dean of the Graduate School. It is understood that any copying or publication or any other use of this thesis or part thereof for financial gain shall not be allowed without my written permission. It is also understood that due recognition shall be given to me and to the University of North Dakota in any scholarly use which may be made of any material in my thesis.

Signature _____

Date _____

TABLE OF CONTENTS

LIST OF FIGURES	vi
LIST OF TABLES	ix
ACKNOWLEDGMENTS	x
ABSTRACT	xi
CHAPTER	
I. INTRODUCTION	1
II. OBSERVATIONAL DATA SET	4
III. AEROSOL – CLOUD CONDENSATION NUCLEI (CCN) CONCENTRATION CLOSURE.....	11
Introduction.....	11
Theory.....	12
Laboratory Data Analysis	15
Field Data Analysis	23
Ground-based CCN Closure	23
Airborne CCN Closure	27
Discussions	31
Conclusions.....	33
IV. AEROSOL – CLOUD DROPLET NUMBER CONCENTRATION (CDNC) CLOSURE.....	35
Introduction.....	35
Theory.....	35
Methodology	37
Results and Discussion	42
Conclusions.....	48
REFERENCES	50

LIST OF FIGURES

Figure	Page
1.	UND-lab setup showing the measurement instruments. An aerosol generator unit, CCNC, PCASP, CPC, and M300 data acquisition system used throughout the experiment. For the front view of the CCNC please refer to the Fig 2, where the same counter was deployed in the aircraft cabin.5
2.	The aircraft platform of the Saudi-09 campaign and close-up views of the instruments. This visual is used by the courtesy of David J. Delene.....7
3.	Relation between dry particle diameter and critical SS in the range of 25 to 100 nm for three κ values. This figure is based on the Figure 1 in Petters and Kreidenweis 2007.14
4.	Time series representation of AS aerosol measured by CCNC, PCASP and CPC instruments as noted by different colors. The data were collected on 25 February 2009 (Feb25). The supersaturation settings of the CCNC are shown by the labels above the time series plot in the 0.2 to 1.0 % range.16
5.	Size resolved PCASP aerosol concentrations for the 25 February 2009 laboratory data. Squares represent average measurements in each bin, while vertical bars show ± 1 standard deviation. Data points are at the channel's geometric mean diameter and the dashed line shows the limits of each channel.17
6.	Size resolved CCN concentrations. The legend lists the colors associated with each SS measurement. The actual diameter range lies in 0.5 to 10.0 μm with a bin increment of 0.5 μm (except the first two channels), but x-axis upper limit cut at 7 μm for ease of view.....18
7.	Number-size distribution function of discrete PCASP and CPC combined aerosol data and best log-normal fit (green line) using the 1.0% supersaturation corresponding time interval on 25 February 2009 case. Squares show the averaged data, while vertical lines show ± 1 standard deviation of discrete aerosol data. Dark and lighter gray margins around the green fitting line show ± 1 and ± 2 standard deviations of fitted aerosol size distribution, respectively.20

8.	Cumulative size distribution representation of fitted and combined aerosol concentration data in Fig. 7.....	21
9.	Measured and calculated CCN concentration comparison for the 25 February 2009 laboratory data. Each supersaturation (SS) measurement is grouped by different colors as given in the upper left located legend. The straight black line shows 1-to-1 correspondence, whereas the straight gray line shows the best linear fit on all plotted data with the equation given on the right along with the coefficient of determination result of the comparison. Dark and light shaded areas show 25% and 50% above the 1-to-1 line.	22
10.	Twomey power-law based CCN concentration estimations and curve-fits constructed based on the most optimum C and k parameters estimated from ground-based CCN concentration spectra. This figure includes the ground CCN closure case (Apr02 – bottom left panel) and five other cases.	25
11.	Variation of CCN ratio over the range of the six different κ assumptions. In the box-and whiskers plots, red lines show the median of ratios, lower and higher ends of the boxes show 25% and 75% percentile of the data, whiskers denote the range of the data, and flier points (blue plus signs) show outliers.	26
12.	Box-and-whiskers plot representation of the CCNC, PCASP and CPC data for all the cases that are given in Table 6.....	30
13.	Time-series representation of the CCNC, PCASP and CPC data for the time-intervals specified in Table 6, for the upper panel shown Apr06 and the lower panel Apr12 cases.	31
14.	Twenty minutes time-series from 13:33:20 – 13:53:20 UTC on the 02 April 2009 aircraft flight. The yellow and gray shaded regions are the cloud-base and in-cloud sampling periods, respectively. The top panel shows the pressure altitude. The middle panel shows the ambient air temperature (blue line) and the dew point temperature (green line). The bottom panel shows the 0.61% supersaturation Cloud Condensation Nuclei (CCN) concentration (blue line) measured with a Droplet Measurements Technology counter, the total (approximately 0.1 to 5.4 μm diameter) optical aerosol concentration (green line) measured by a model 100 Passive Cavity Aerosol Spectrometer Probe (PCASP), and the Condensation Nuclei (particles larger 10 nm in diameter) concentration measured by a TSI Condensation Particle Counter model 3772.....	38
15.	Similar to the Fig. 14, except the top panel shows the DMT Hotwire liquid water content (LWC), the middle panel shows SPP-100 model FSSP cloud droplet concentration, and the bottom panel shows the Sky Avionics Ball variometer vertical velocity.....	39

16. The top panels show normalized histograms (binned in 10 intervals) of the cloud-base and in-cloud updrafts (for $w > 0$). Average updrafts for the presented section are also noted with $\langle w \rangle$ notation. The bottom-left panel shows cloud-base normalized average PCASP aerosol spectra. Normalized ± 1 standard deviation aerosol spectra are overlaid on the average step plot using vertical lines. The bottom-right panel shows supersaturation spectrum based on the 0.61% supersaturation measurement and the k parameter value obtained from pre-flight surface CCN spectrum measurements.....40
17. Activation spectra of the accumulation-coarse and Aitken mode aerosol. The accumulation-coarse mode spectra are based on the average cloud-base PCASP aerosol measurements from the Apr02 flight and $\kappa = 0.1$ and 1.0 hygroscopicity assumption as drawn by red and blue colors, respectively. Aitken mode spectra is constructed from the power-law fit as described in the methodology section.41
18. Vertical SS profiles as experienced in the parcel model with the four distinct initialization conditions noted in the upper-right corner of the figure.42
19. Comparisons of the parcel model predicted N_d (shown with blue and red histograms) and the FSSP measured N_d (the same black histogram in each panel). Predicted average N_d is noted for each case with $\langle N_d \rangle$ notation. The average in-cloud observed N_d is 223 cm^{-3} for all cases.44
20. Growth history of four different setting initialized 15 accumulation/coarse and 12 Aitken mode aerosol. Note that $w = 1.27 \text{ m s}^{-1}$ corresponds to the average updraft velocity in the cloud-base while 4.37 m s^{-1} is the maximum updraft observed in cloud-base. The cross-sections of the gray lines notes the maximum particle size reached within the parcel. The bottom two panels note the elapsed times until the parcels reach to the specified end-pressure point.....45

LIST OF TABLES

Table	Page
1. Aerosol-CCN closure study data set.	10
2. Aerosol-cloud droplet closure study data set.	10
3. Statistical results of the laboratory data analysis.	23
4. Part 1 of Apr02 ground data statistics and analysis results.	24
5. Part 2 of Apr02 ground data statistics and analysis results.	26
6. Part 1 of the airborne data statistics and analysis results. Note that all CCN concentrations are reported at 0.61% SS setting.	27
7. Part 2 of the airborne data statistics and analysis results. Note that all CCN closure calculations are performed at 0.61% SS setting.	29
8. Overall statistical results of the airborne CCN closure.	30
9. Cloud droplet number concentration comparison of 12 different way initialized parcel model runs. Note that the cloud-base measured average PCASP concentration ($\langle \text{PCASP} \rangle$) is 284 cm^{-3} with the standard deviation of 96 cm^{-3}	46

ACKNOWLEDGMENTS

I am grateful to my advisor Dr. David J. Delene for his continuous support not only in performing this study, but also throughout my graduate education. My thesis committee members; Drs. Michael R. Poellot and Jianglong Zhang have provided valuable comments and discussions for improving the quality of the scientific work and making me a better writer. Special thanks go to Dr. Jefferson R. Snider for allowing me to experiment with his model and providing me a new opportunity to continue my curious investigations in the wondrous worlds of clouds.

ABSTRACT

A cloud condensation nuclei (CCN) closure study is performed to test our theoretical understanding between aerosol properties and the cloud nucleating ability of aerosols. Thermodynamic and microphysical evolutions of cloud aerosol are also investigated within a cloud droplet number concentration (N_d) closure study by running adiabatic parcel model simulations in warm, non-precipitating cloud development. Ground and airborne aerosol, cumulus cloud microphysical, and atmospheric state measurements from the Saudi Arabia Spring 2009 field campaign are used in both closures, with the exception that the CCN closure is first established utilizing idealized laboratory data collected in the University of North Dakota. In the idealized case, CCN concentrations, that are obtained from unimodal log-normal aerosol size-distribution and employing the κ -Köhler theory with the well-defined hygroscopicity assumption of ammonium sulfate aerosol, over-predicted from 7% to 38% in the increased 0.2 to 1.0% supersaturation range. The κ parameter is varied from 0.6 to 0.1 in field data based CCN closures, and lower soluble values (0.2 ± 0.1) are found giving the best agreement. One parcel model simulation results show that in-cloud droplet number concentrations are predicted within 10% based on average measured and predicted N_d comparison, using below-cloud vertical velocity distributions and $\kappa = 0.1$ initialized aerosol chemical composition assumption. Unlike in marine stratus cloud closure studies, this cumulus based N_d closure cannot be achieved by using a characteristic (average) cloud-base updraft profile. The $\kappa = 1.0$ set model run strikingly reveals that, even though resulting

in 2% under-prediction of N_d , final cloud droplet sizes reach about 15.3 μm in radius comparing to 10.7 μm in the $\kappa=0.1$ simulation. Implications of this apparently small 4.6 μm difference might provide guidance in modifying the micro-structure of the studied region clouds for improved precipitation efficiencies.

CHAPTER I

INTRODUCTION

Aerosol-cloud-climate interactions have been in greater focus within the atmospheric research community and related disciplines over the last few decades (e.g., Hobbs 1993, Lohmann and Feichter 2005, IPCC 2007, Andrea and Rosenfeld 2008, Levin and Cotton 2008). Regardless of whether they actually form clouds or not, understanding of aerosols has significant implications to establish and resolve the feedback mechanisms of the complex aerosol-cloud-climate chain. Aerosols can directly or indirectly affect the radiative and thermodynamic energy budgets of the atmosphere, cause short and long term warming and cooling in the global climate, and perhaps more importantly, they can inadvertently or artificially alter the precipitation development processes in clouds.

The cloud forming ability of aerosols has been typically scrutinized in the form of aerosol-cloud condensation nucleus (CCN) closure studies to understand and improve our theoretical knowledge of the thermally, physically and chemically coupled interactions and instrumental measurement procedures. Among the performed CCN closures, Covert et al. (1998) report a ground-based single point supersaturation (SS) measurement based study, VanReken et al. (2003) describe an airborne two point SS measurement based marine study, and Broekhuizen et al. (2006) report a ground-based single point SS measurements based CCN closure using full aerosol size spectra and simultaneous chemical composition measurements. Results of the closure agreement varied depending on the source of the aerosol sampled (i.e., natural – anthropogenic, pristine – polluted),

type of the measurements used (i.e., continuous flow CCN chamber, static growth chamber, partial – full aerosol size spectrum), and the classifications of the clouds studied (i.e., cumulus – stratiform), with additional assumptions regarding the chemical state of the sample aerosols.

The further analyses in the microphysical, thermodynamical and physicochemical aerosol-cloud interactions, i.e., the evolution of aerosols to cloud droplets, are investigated within the context of aerosol-cloud droplet number concentration (CDNC - N_d) closure studies. Starting with as early as Twomey (1959) simple analytical equations based, adiabatic parcel model based (Snider et al. 2003), and detailed cloud droplet activation parameterization scheme (Fountoukis and Nenes 2005) based predictions of N_d were compared and contrasted to observed measurements of CDNC. Varying degree of closure assessments have been made in these studies based on the measured aerosol and CCN concentrations, cloud-base vertical velocity (w) measurements, and the chemical composition of the aerosol. Although uncertainties from the CCN closure step propagate through the aerosol-CDNC closure, these uncertainties are suppressed by almost 50% in the cloud droplet closure as demonstrated in the work of Sotiropoulou (2006).

In the first part of this thesis a CCN closure study is performed and its usefulness and feasibility tested without having full-scale aerosol diameter size spectra and particle chemical composition information. CCN closure is said to be achieved when predicted values of CCN concentrations are comparable to those of measured values. In this study, predictions of CCN concentrations are made by using measured particle size information and by utilizing the Köhler theory with and without making assumptions about chemical composition of measured aerosols. These results are compared to measurements made by

a CCN counter. Previous studies suggest that assumption of a typical aerosol composition has much less impact on the prediction of cloud nucleating ability of aerosols than having a typical size distribution assumption (e.g., Dusek et al. 2006). Along these lines, CCN closure studies examine the validity of this assumption by employing a single parameter representation of hygroscopic growth activity which accounts for the solute effect of an aerosol particle in the alternative form of the original Köhler equations as expressed by κ -Köhler theory. The data set for this study includes Condensation Nuclei (CN) concentrations from a Condensation Particle Counter (CPC), aerosol concentrations for 0.1 to 3.0 μm diameter particles from a Passive Cavity Aerosol Spectrometer (PCASP), and CCN concentrations from a Droplet Measurements Technologies (DMT) CCN counter. These data were collected during the Spring 2009 Saudi Arabia field campaign and in laboratory experiments performed in the University of North Dakota.

The second part of the thesis follows with another closure study to predict cloud droplet number concentration from a given aerosol number concentration and prescribed cloud-base updraft velocity. In addition to the airborne data that are used in the first section, measured cloud droplet concentrations are used from a Forward Scattering Spectrometer Probe (FSSP). Updraft velocity estimations are obtained from a Sky Avionics Ball Variometer probe. Prediction of the cloud droplet concentrations is performed with an adiabatic cloud parcel model. The derived aerosol size distribution and estimated chemical composition and updraft velocities from a single case cloud-base and first in-cloud pass measurements of non-precipitating and non-seeded cumuliform cloud are inputted into the model to predict N_d .

CHAPTER II

OBSERVATIONAL DATA SET

The aerosol – Cloud Condensation Nuclei (CCN) and aerosol – cloud droplet concentration closure studies were performed with data sets from experiments conducted in the University of North Dakota Department of Atmospheric Sciences laboratory (UND-lab) and during the Spring 2009 Saudi Arabia (Saudi-09) field campaign. The UND-lab data set provides an effective way to test the aerosol – CCN concentration closure study hypothesis due to the controlled conditions of the laboratory environment and the known chemistry of the sampled aerosol. For this reason, the aerosol – CCN closure experiment is first tested on laboratory data and further extended using the Saudi-09 data set. The aerosol – cloud droplet closure study extensively uses the airborne data set since no laboratory data is available due to the difficulties of reproducing the necessary atmospheric conditions in the lab.

The UND-lab experimental setup is shown on Fig. 1. An aerosol generator is used to atomize an Ammonium Sulfate $[(\text{NH}_4)_2\text{SO}_4]$ solution (1 g L^{-1}) to create particles which are subsequently dried using a diffusion dryer. The air stream is split and sampled by a Droplet Measurements Technologies (DMT) CCN counter, a Particle Measuring Systems (PMS) model 100 Passive Cavity Aerosol Spectrometer Probe (PCASP) and a TSI Incorporated model 3771 Condensation Particle Counter (CPC). The CCN counter grows particles by diffusional growth in its chamber under a set supersaturation condition and an optical particle counter, located at the exit of the chamber, counts droplets that are

between 0.75 to 10 μm in diameter. The DMT CCN counter is a commercialized version of the continuous flow CCN chamber described by Roberts and Nenes (2005). Supersaturation (SS) calibration of the counter was performed at DMT in July 2008, while pressure and flow calibrations were conducted in the lab to ensure the quality of the CCN measurements.

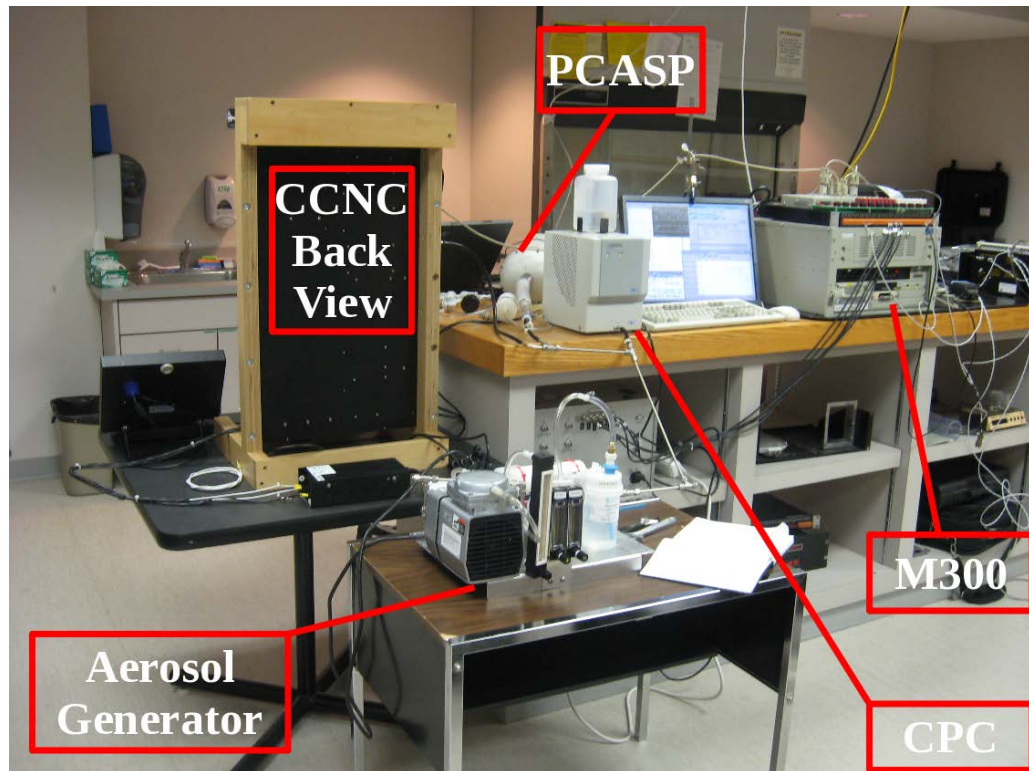


Figure 1: UND-lab setup showing the measurement instruments. An aerosol generator unit, CCNC, PCASP, CPC, and M300 data acquisition system used throughout the experiment. For the front view of the CCNC please refer to the Fig 2, where the same counter was deployed in the aircraft cabin.

The PCASP sizes particles one at a time as they pass through its sampling volume by measuring the amount of scattered light. Particles are sized into 15 channels between theoretical limits of 0.1 to 3.0 μm in diameter; channel size boundaries are based on individual instrument performance and measurement characteristics (Garvey and Pinnick 1983). In this study, size boundaries of the PCASP are calculated by applying

calibrations conducted with 222 nm latex microsphere polystyrene beads from Duke Scientific (<http://www.dukescientific.com>). The polystyrene beads have a real refractive index of 1.59 at 589 nm, while ammonium sulfate has a real refractive index of 1.525 and an imaginary refractive index of $1e-7$ at 656 nm (Toon 1976). The calibration processing software (Delene 2010) uses the ammonium sulfate refractive index when determining the channel sizes.

The CPC grows particles ≥ 10 nm in diameter to detectable size by diffusional growth, using butanol as the condenser liquid. Particles are counted by an optical particle counter based on the detection of the scattered light (TSI Inc. 2007). The instrument was operated with a critical orifice tied to a pump through a plastic tubing to maintain a constant mass flow.

Both for the UND-lab and Saudi-09 data sets, all instrument data was acquired by the Science Engineering Associates (SEA) M300 data acquisition system. The Airborne Data Processing and Analysis (ADPAA) software package (Delene 2010) was used to process the recorded data. Instrumental delays (e.g., the PCASP measures the particles quickly whereas the CCN counter requires certain growth time, and measurements by in-cabin instruments lag those of probes located under the wings in the free air stream) have been adjusted by shifting the required data appropriately in time. Correlation analysis of the collected data indicates that the CCNC measures the particles after an approximate 15 seconds delay comparing to the PCASP, under the default 0.5 L min^{-1} flow rate setting.

The Saudi-09 data set was collected in Saudi Arabia, Riyadh region between 15 March – 15 April 2009. Figure 2 shows the Raytheon Beechcraft King Air 200 aircraft and the research instruments used throughout the campaign. In addition to the

instruments used in the UND-lab data set, a DMT Forward Scattering Spectrometer Probe ([FSSP] model 100 with Signal Processing Package [SPP] upgrade) and a Sky Avionics Ball Variometer (BallVario) were deployed for extensive characterization of the aerosol and cloud properties in the region. The FSSP is a common instrument that obtains the cloud droplet size distributions (3 – 47 μm in diameter in 20 channels) by measuring the intensity of scattered light of the particles that pass through a laser light beam (Dye and Baumgardner 1984). The device calibration was performed using 30 μm beads and performance checks were done after each flight due to the dusty conditions in Saudi Arabia (Delene et al. 2009). The BallVario provided three-dimensional wind measurements, particularly below and in cloud updraft velocities. Delene et al. (2009) describes the Saudi-09 data set in more detail providing information regarding additional instruments that are not explicitly represented in this text.

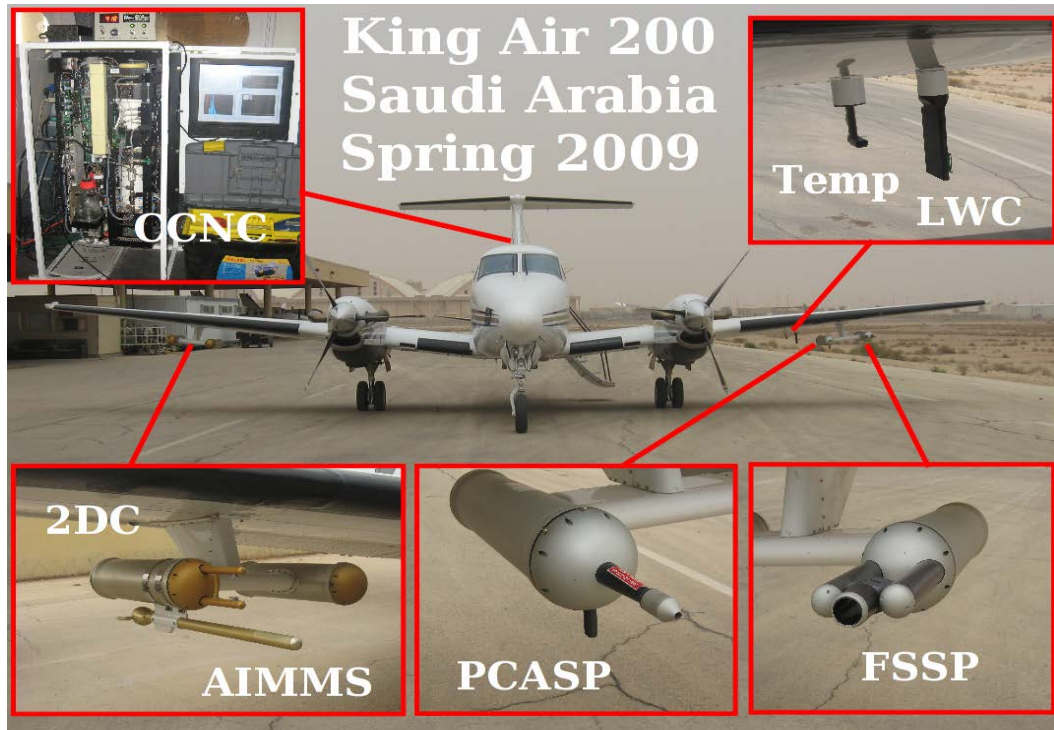


Figure 2: The aircraft platform of the Saudi-09 campaign and close-up views of the instruments. This visual is used by the courtesy of David J. Delene.

An Inlet Pressure Controller (IPC) unit (DMT – SN: 0608-0018) was used on all flights and most of the ground measurements. This device maintains a constant chamber pressure for the CCN counter to minimize pressure fluctuations and variations in the device SS, therefore providing stable airborne CCN measurements. Typically, the IPC was set at 500 mb during the lab experiments, and set to 425 mb for the Saudi-09 campaign. Rose et al. (2008) reported a 0.037% change in the effective SS per 100 mb at 5 K temperature gradient at 0.5 L min⁻¹ flow rate settings. DMT (2007) reported a 0.07% change in the effective SS per 100 mb change in the pressure based on the calibrations performed at 830 mb in Boulder, Colorado, USA. The CCNC supersaturation reported in this study is adjusted for the aforementioned pressure variation. Routine flow and pressure calibrations and pressure leak tests were performed on the counter in order to obtain high quality CCN data. During the March 23, 2009 test, the counter was observed to leak less than 0.2 mb min⁻¹, very low values, when the instrument was installed on the aircraft (Delene and Sever 2009).

A reverse-facing 314 stainless steel 0.25 inch diameter inlet was used to transport air into the CCNC and CPC which were in the aircraft's cabin. The inlet was exposed to droplet splash effect during cloud penetrations; however, this study only uses out of cloud measurements based on a Hot Wire probe measured liquid water content threshold (0.05 g m⁻³) to clearly distinguish cloud-free or in-cloud regions in the analysis intervals.

Runjun Li (Personal Communication) performed a post-field SS calibration while the counter was set at 600 mb in Saudi Arabia before the instrument was removed from the aircraft. His calibration procedure followed the description given in Rose et al. (2008) (i.e., step-wise incrementing through the temperature gradient for selected dry

ammonium salt particles, measuring the total and activated aerosol concentrations, and later obtaining effective SS's for each temperature gradient.) The results of the calibration indicated that the CCN counter was running at approximately 25% below the instrument reported SS value during Saudi-09. This difference could be attributed to long distance shipment of the instrument, the varied environmental conditions under which the calibrations were performed, or build up of material on the inside walls of the counter. Furthermore, this difference illustrates the importance of in-field calibrations of the DMT CCN counter when operated on airborne field project. The field calibration was applied to the Saudi-09 data set to take into account observed change.

Table 1 and Table 2 give details on the three main categories of data sources used in this study: 1) Laboratory (Lab), 2) Ground, 3) Airborne. Ground data are surface measurements obtained in Riyadh, Saudi Arabia using the same aircraft platform as the airborne measurements, while Lab data were obtained at UND before the start of the field project. A few cases on Tables 1 and 2 could intersect for the use of aerosol – cloud droplet study since CCN spectra are needed to construct Aitken mode aerosol spectra for the cloud parcel model initialization. Details of the instrument data and exact analysis intervals are given in the subsequent chapters and these two tables should be used in conjunction with the information provided in Chapters 3 and 4.

Apart from the instruments listed in Tables 1 and 2 (right column), data from temperature and pressure sensors were used to normalize CCN counter measurements to ambient pressure and temperature. This correction is required because the instrument chamber pressure was kept less than or equal to 500 mb and temperature values at the exit of the chamber were greater than ambient temperature. PCASP and FSSP

measurements were made at ambient condition, therefore no correction is necessary. Throughout this work the CN, CCN and SS values are reported at ambient conditions. Thus, atmospheric state parameter measurements (e.g., temperature, dew-point temperature, pressure) play an important role in analyzing the aerosol and cloud properties. They are also used in this study to initialize the cloud parcel model that is used in the aerosol – cloud droplet concentration closure study section (Chapter 4). The CCNC was run at a single SS setting in airborne operations and the required cloud base level SS's are extrapolated using the ground SS spectrum measurements.

Table 1: Aerosol-CCN closure study data set.

Data File ID	Source	Duration*	Instruments: Model / Serial #
20090210_203159	Lab	8:08:30	CCNC-100 / 062 PCASP-100X / 30013-1191-11 CPC-3771 / 70827077
20090224_215058	Lab	3:21:00	
20090225_011651	Lab	2:17:14	
20090225_034214	Lab	1:10:56	
20090402_115619	Ground	0:28:57	CCNC-100 / 062 PCASP-100X / 19610-0590-06 CPC-3772 / 70907298
20090402_131020	Airborne	2:32:47	
20090406_130109	Airborne	2:54:05	
20090408_123026	Airborne	2:20:51	
20090409_123225	Airborne	1:55:17	
20090412_115713	Airborne	3:11:48	

* These are total recording lengths (in HH:MM:SS notation) for each particular data file. Only time segments during which a valid combination of the CPC, PCASP and CCNC data exist are used in the analysis.

Table 2: Aerosol-cloud droplet closure study data set.

Data File ID	Source	Duration*	Instruments: Model / Serial #
20090402_131020	Airborne	2:32:47	CCNC-100 / 062 PCASP-100X / 19610-0590-06 FSSP-100 / 1947-0281-60 Ball Variometer / NA Hygrometer / NA

* Analysis intervals restricted with cloud-base and the consequent in-cloud samplings.

CHAPTER III

AEROSOL - CLOUD CONDENSATION NUCLEI (CCN) CONCENTRATION CLOSURE

Introduction

A Cloud Condensation Nuclei (CCN) closure was performed utilizing κ -Köhler theory (Petters and Kreidenweis 2007, Petters and Kreidenweis 2008) and single mode two-parameter –geometric mean diameter (gm), geometric standard deviation (gsd) lognormal least squares fitting approach using datasets collected in laboratory and the field campaign described in Chapter 2. In the laboratory experiments, well-studied ammonium sulfate (AS) aerosol run through the CPC, PCASP and CCNC instruments and closure were tested by using a $\kappa=0.6$ assumption of AS for 0.2 to 1.0% varying supersaturation (SS) conditions. Compared to the laboratory experiments, the field data analysis (both from ground-based and airborne measurements) followed a different approach. Here, κ hygroscopicity parameter was varied from 0.6 to 0.1 for the selected ground and cloud-base measurement portions and unimodal lognormal fits constructed on the analysis intervals. This approach was followed mainly because the field datasets do not have direct measurement regarding the chemical composition or growth factor of the measured aerosols. Varying the κ and achieving the most optimum closure gives a rough estimation regarding the hygroscopicity of the particles in the studied region.

The next section describes the κ -Köhler theory and estimation of critical activation diameter for a given SS, κ value, and unimodal lognormal fitting function. Later,

laboratory and field analysis sections explain the details of closure studies. Following that, a discussion section highlights the important points that affect achieving closures or problems that were encountered within each analysis. Finally, conclusions summarize the unexpected and expected findings of the study.

Theory

Köhler theory (Köhler 1936) explains the relations between the physicochemical properties (i.e., size and composition) of a particle to the saturation ratio or excess of saturation (i.e., SS) to activate the particle. One of the general forms of the Köhler equations is shown in Eq. 1 (Adopted from Eq. 6-29 in Pruppacher and Klett 1997, and Roberts and Nenes 2005).

$$S_{eq} = 1 + \frac{A}{r} - \frac{B}{r^3} \quad (1)$$

$$A = \frac{2 M_w \sigma_{s/a}}{\mathcal{R} T \rho_w} \approx \frac{3.3 \times 10^{-5}}{T}, \quad B = \frac{3 \nu m_s M_w}{4 \pi M_w \rho_w} \approx \frac{4.3 \nu m_s}{M_s} \quad (2)$$

where S_{eq} is the equilibrium saturation ratio, r is the particle radius, M_w is the molar mass of water, $\sigma_{s/a}$ is the surface tension of the solution/air interface, \mathcal{R} is the universal gas constant, T is temperature, ρ_w is the density of water, ν is the total number of ions per dissociating molecule, m_s the mass of solution, M_w is the molar mass of the water, M_s is the molar mass of the solute. Here, the two opposing terms; $\frac{A}{r}$ represents the Kelvin effect (i.e., the surface tension of a droplet) and $\frac{B}{r^3}$ represents the Raoult effect (i.e., the dissolved solute term). As it is explicitly shown in the equation, solving for a particular critical SS requires knowing detailed information regarding the chemical composition of a given particle.

In an alternative approach proposed by Petters and Kreidenweis (2007), chemical

composition, or water uptake ability of a particle, is represented by a single κ -hygroscopicity parameter. The κ -Köhler version of the Köhler equation is shown in Eq. 3.

$$S(D) = \frac{D^3 - D_d^3}{D^3 - D_d^3(1-\kappa)} \exp\left(\frac{4 M_w \sigma_{s/a}}{\mathcal{R} T \rho_w D}\right) \quad (3)$$

where D is the diameter of the droplet, D_d is the dry diameter, and κ is the hygroscopicity parameter.

The relation between dry particle diameter and critical SS is easily determined for κ of 0.6, 0.4 and 0.2 as shown in Fig. 3, assuming $\sigma_{s/a} = 0.072 \text{ J m}^{-2}$ and $T = 298.15 \text{ K}$ as was done in Petters and Kreidenweis (2007). Throughout the study, $\sigma_{s/a}$ and T were kept constant in calculating critical activation diameter (D_c). In this framework, a κ value of 1.2 is representative of a highly soluble particle (e.g., NaCl), a κ value of 0.6 for a soluble particle (AS), and 0.1 for a low soluble particle. As it is seen from Fig. 3, the effect of κ decreases when the size of a particle increases. Also apparent from Fig. 3 is that larger sized particles require lower SS to be activated or grow further to become a cloud droplet in this study's context. One can numerically calculate the required SS from a given dry particle using Eq. 3 or alternatively using the graphical estimations shown in Fig. 3.

Another important theoretical consideration to calculate predicted CCN amount is to provide a size distribution space of measured aerosol. Throughout the study, a two-parameter (gm, gsd) single mode log-normal distribution is used to represent measured aerosols. Equation 4 shows the version of a log-normal function used in this study. (Eq. 8.33 in Seinfeld and Pandis 2006)

$$\frac{dN}{d\text{Log}D_p} = \frac{N_t}{(2\pi)^{1/2} D_p \text{Log}\sigma_g} \exp\left(-\frac{(\text{Log}D_p - \text{Log}\bar{D}_{pg})^2}{2\text{Log}^2\sigma_g}\right) \quad (4)$$

where N_t is the total aerosol number concentration, \bar{D}_{pg} (gm) is the geometric mean

diameter, σ_g (gsd) is the geometric standard deviation of the log-normal distribution. $\text{Log}(x)$ is used for natural base logarithm or $\text{Ln}(x)$. Aerosol concentration normalization is done in various forms (e.g., dN/dD_p , $dN/d\text{Log}10D_p$). The $d\text{Log}D_p$ normalized form of the aerosol is used here, primarily because PCASP size channels are logarithmically spaced in size domain.

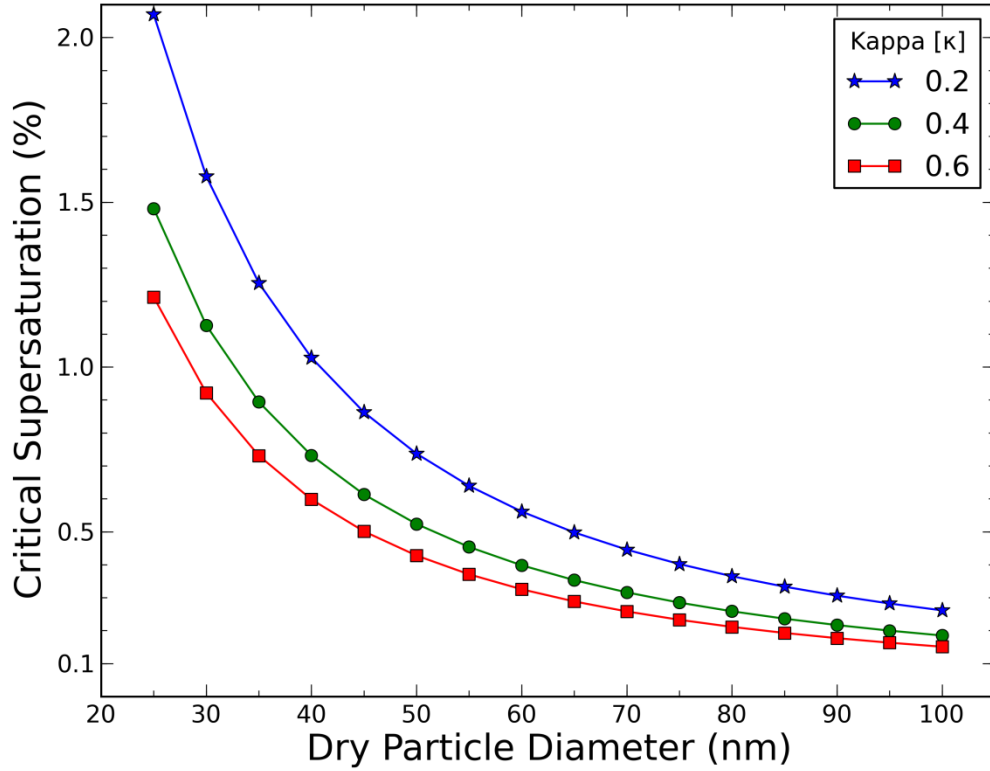


Figure 3: Relation between dry particle diameter and critical SS in the range of 25 to 100 nm for three κ values. This figure is based on the Figure 1 in Petters and Kreidenweis 2007.

In the atmosphere, aerosol distribution is typically represented by the summation of multi-modes as shown in Eq. 5:

$$\frac{dN}{d\text{Log}D_p} = \sum_{i=1}^n \frac{N_i}{(2\pi)^{1/2} D_p \text{Log}\sigma_i} \exp\left(-\frac{(\text{Log}D_p - \text{Log}\bar{D}_{pi})^2}{2\text{Log}^2\sigma_i}\right) \quad (5)$$

where variables are the same as in Eq. 4, except N_i is the number concentration, \bar{D}_{pi} is the

mean diameter, and σ_i is the standard deviation of i^{th} lognormal mode. The main idea behind representing aerosol population using a lognormal fit is to describe the aerosol data with the least amount of points (N_i , gm, gsd) instead of using discrete size spectra obtained from size spectrometers. The datasets used in this study do not have full aerosol size spectra measurements, and one of the tests in this study was to perform and assess CCN closures using a single modal aerosol distribution assumption.

Laboratory Data Analysis

The laboratory data based CCN closure study was performed using four tests. The first 25 February 2009 (hereafter, Feb25 for brevity) test used five different SS values and was selected to describe the details of the analysis procedure. Detailed exploratory plots (Figs. 4 through 9) were created using this test and are not re-shown for the other studied cases. Figure 4 shows time series representation of PCASP, CPC, and CCNC measured aerosol and CCN data. As shown from the step behavior of the CCN measurements, the counter was run in spectra mode cycling through SS in the 0.2 to 1.0% range. The CPC measures the concentration of particles 10 nm in diameter and above, which is usually referred to as total aerosol number concentration.

The PCASP measured number concentration is obtained by using size spectra measurements that are done in 15 binned channels. The unnormalized concentration plot in Fig. 5 shows a sample size spectral measurement. As described in Fig. 5, squares represent the average aerosol measurement, whereas vertical lines show one standard deviation above and below the data distribution. For 1 g L⁻¹ of AS solution, concentration drops to zero, near-zero values around 0.5 μm diameter size threshold. A step-wise plot is overlaid in Fig. 5. This depiction better represents the discrete nature of

measurements and also better shows the channel size limits, while in the line and discrete plot cases, data points are located in the geometric mean of each channel interval. In this laboratory experiment, the channel size limits of PCASP were determined as 0.0897, 0.1097, 0.1292, 0.1588, 0.1872, 0.2295, 0.2670, 0.3668, 0.4448, 0.6201, 0.8494, 1.1691, 1.2903, 1.5512, 2.2704, 2.6850 μm .

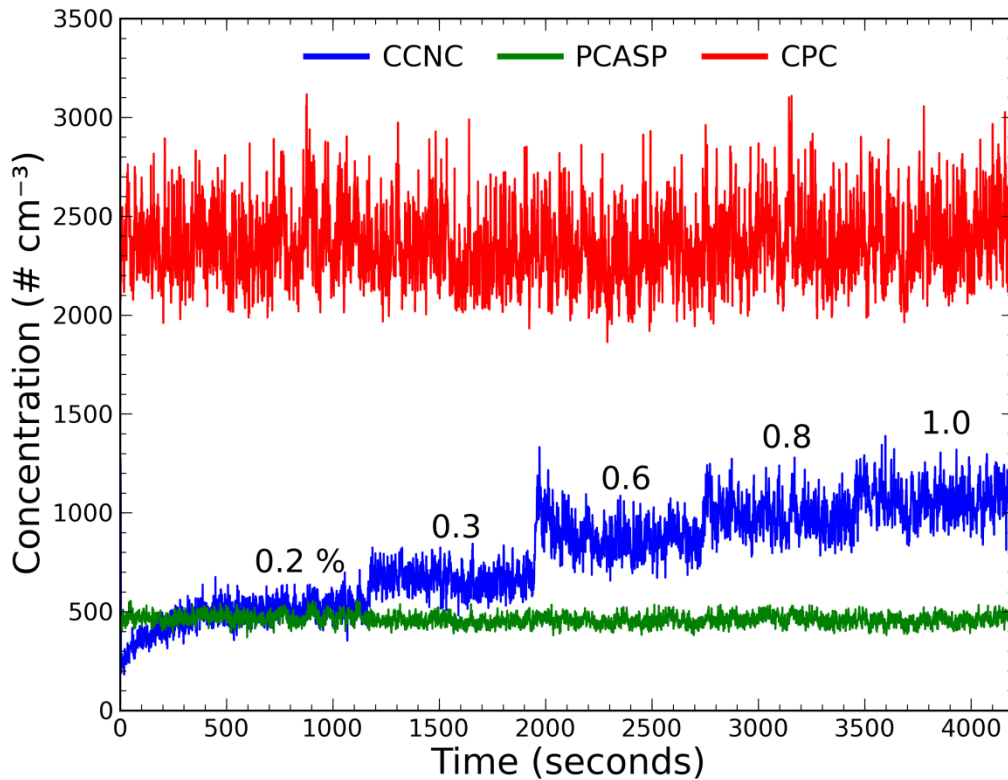


Figure 4: Time series representation of AS aerosol measured by CCNC, PCASP and CPC instruments as noted by different colors. The data were collected on 25 February 2009 (Feb25). The supersaturation settings of the CCNC are shown by the labels above the time series plot in the 0.2 to 1.0 % range.

CCNC measures activated aerosol particles in 0.75 to 10.0 μm in diameter ranging over 20 channels. Figure 6 shows the average CCN size spectra obtained in Feb25 case. The most notable features of these size-spectra plots are 1) with the exception of 0.2 and 0.3% SS measurements peak mode size shifts to the right with increasing SS, 2) the

breadth of modes gets narrower in the increasing SS direction. The reason for the peak mode shift is that in higher SS environments, particles experience greater diffusional growth. The peak mode narrows because the relative growth due to condensational growth decreases with increasing particle sizes, thus causing narrower spectral distributions at higher SS settings.

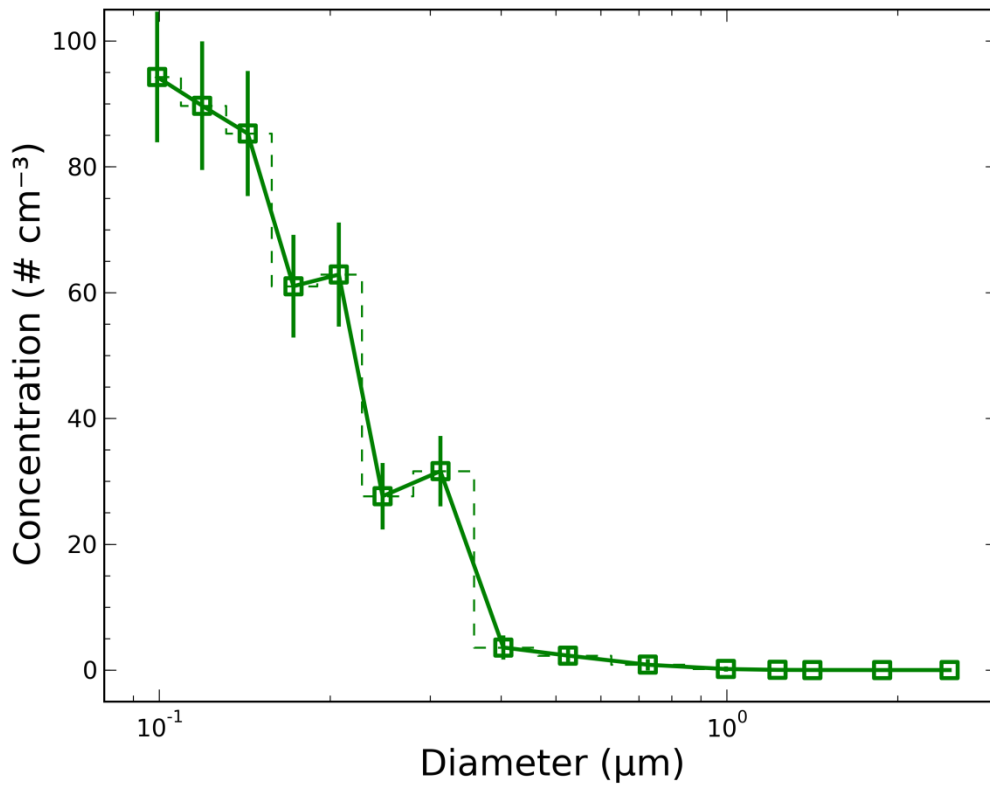


Figure 5: Size resolved PCASP aerosol concentrations for the 25 February 2009 laboratory data. Squares represent average measurements in each bin, while vertical bars show ± 1 standard deviation. Data points are at the channel's geometric mean diameter and the dashed line shows the limits of each channel.

For 0.2, 0.3, 0.6, 0.8, and 1.0 SS values set at the CCNC, corresponding critical activation diameters (D_c) are calculated as 83, 53, 40, 33, and 29 nm, respectively under $\kappa=0.6$ hygroscopicity assumption of AS aerosol. It is noted that since the PCASP measures particles within 0.09 to 2.69 μm range, and CPC measures all particles above

10 nm, the PCASP measured aerosol spectra is required to be extended toward lower size ranges in order to capture lower D_c points since even the largest D_c is beyond the lowest PCASP channel limit. To overcome this difficulty, PCASP and CPC measurements are combined using the following scheme: 1-) Full PCASP data are acquired, 2-) CPC data are acquired, 3-) the difference between total number concentration and PCASP measured aerosol concentration is assigned to the geometric mean location of 10 and 90 nm (~ 29 nm) based on the unimodal aerosol distribution assumption.

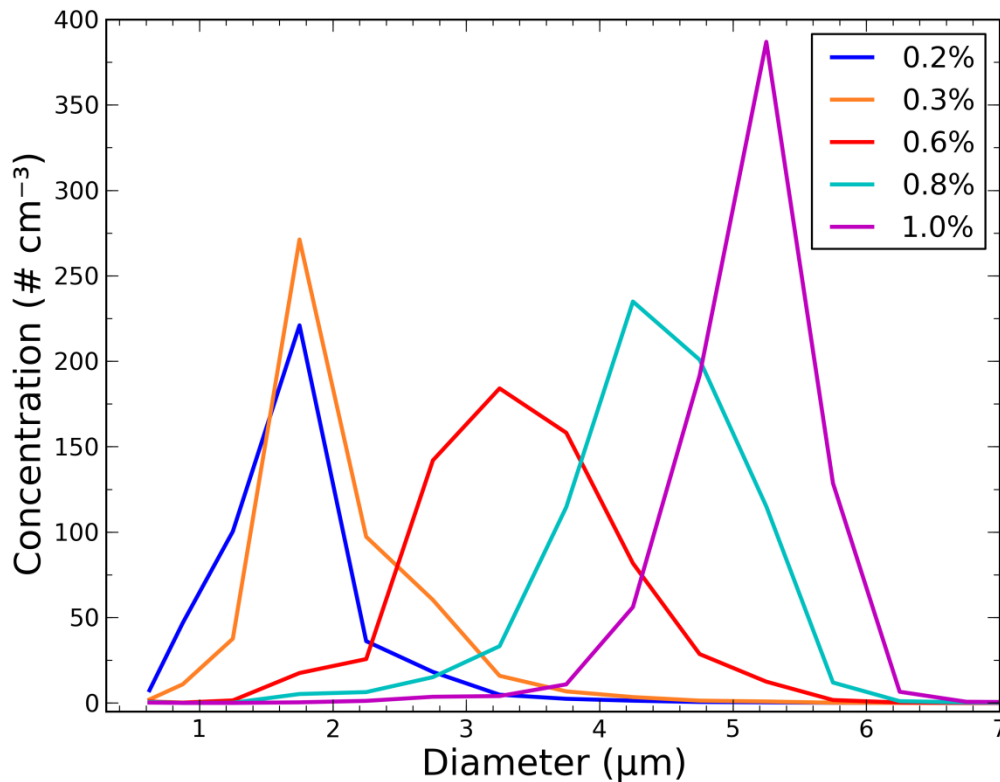


Figure 6: Size resolved CCN concentrations. The legend lists the colors associated with each SS measurement. The actual diameter range lies in 0.5 to 10.0 μm with a bin increment of 0.5 μm (except the first two channels), but x-axis upper limit cut at 7 μm for ease of view.

The next step in the analysis is the construction of lognormal fit on the newly created aerosol size spectra. The previously described lognormal function is fitted on this data

using Levenberg-Marquardt non-linear least squares technique. We use the implementation provided by the SciPy library (SciPy, `scipy.optimize.leastsq`). Here, first, best fitting gm and gsd parameters are obtained from `leastsq` function, then lognormal fit is constructed using the N_t in the diameter space of 1 nm to 2.69 μm (the upper end of PCASP channel limits) with one nm increments. The technique described by Jacobson (2005) was also tested to estimate the most optimum lognormal fitting parameters. However, that method failed to capture discrete data using the same unimodal lognormal distribution assumption. The Levenberg-Marquardt technique gives the best statistical agreement in terms of minimizing the sum of squares of the error between the fit function and data points, thus yielding the best fit.

The demonstration of lognormally fitted data is illustrated in Fig. 7. The demonstration is made using an analysis time interval when the 1.0% SS CCN measurements were stable. Analysis time intervals were determined from CCN measurements, mainly to include stabilized CCN measurements and matching PCASP and CPC segments. As it can be seen on Fig. 4, the beginning of 0.6% and later SS CCN measurement periods suffer from unmaintained chamber SS, resulting in above average spiking data points. This issue becomes even more problematic in harsher operating conditions (e.g., pressure-stabilized cabin, not-well leak tested counter.) Field based CCN measurements are corrected either by automatic detection based on checking the temperature stabilization flag data or manually editing the data in certain situations.

Continuing on the analysis, from the determined time interval 600 seconds data were selected. (Throughout this study and the following CDNC chapter all of the data analyzed are 1 Hz and higher frequency data obtained from different probes are averaged to 1 Hz.)

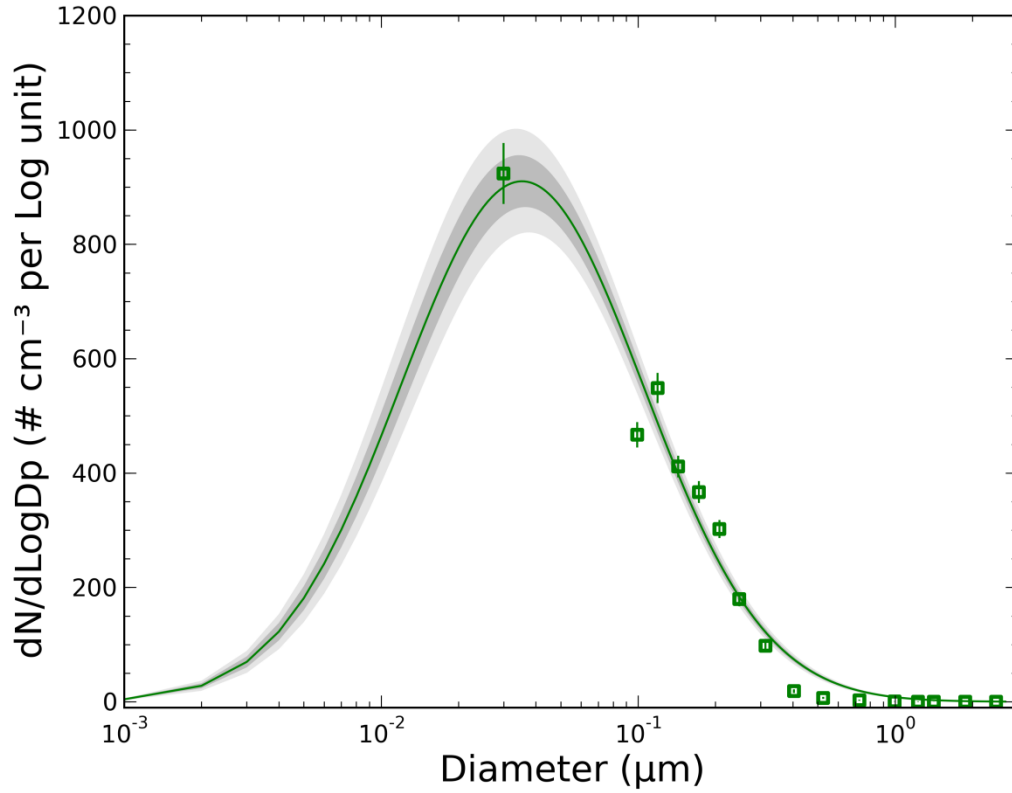


Figure 7: Number-size distribution function of discrete PCASP and CPC combined aerosol data and best log-normal fit (green line) using the 1.0% supersaturation corresponding time interval on 25 February 2009 case. Squares show the averaged data, while vertical lines show ± 1 standard deviation of discrete aerosol data. Dark and lighter gray margins around the green fitting line show ± 1 and ± 2 standard deviations of fitted aerosol size distribution, respectively.

These selected data are further averaged to 1/10 Hz to lower instrumental time sampling differences. For each 10 seconds time interval (60 points), the optimum g_m and g_{sd} values are calculated. Using these data points, the g_m and g_{sd} data pair, average fitting line and ± 1 and ± 2 standard deviation extending shaded areas, are plotted in Fig. 7. Likewise, average and ± 1 standard deviation above and below of discrete aerosol data is constructed from 10 seconds averaged, 600 seconds combined PCASP and CPC data. Once the number-size distribution function is created, the cumulative size distribution function is obtained by cumulatively summing up the fitted or discrete aerosol data and

multiplying the $dN/d\text{Log}D_p$ with the corresponding log bin sizes. Like the example shown in Fig. 8, cumulative size distribution plots are important to show how well the measured aerosol data and best-fit constructed aerosol amounts agree in total number concentration.

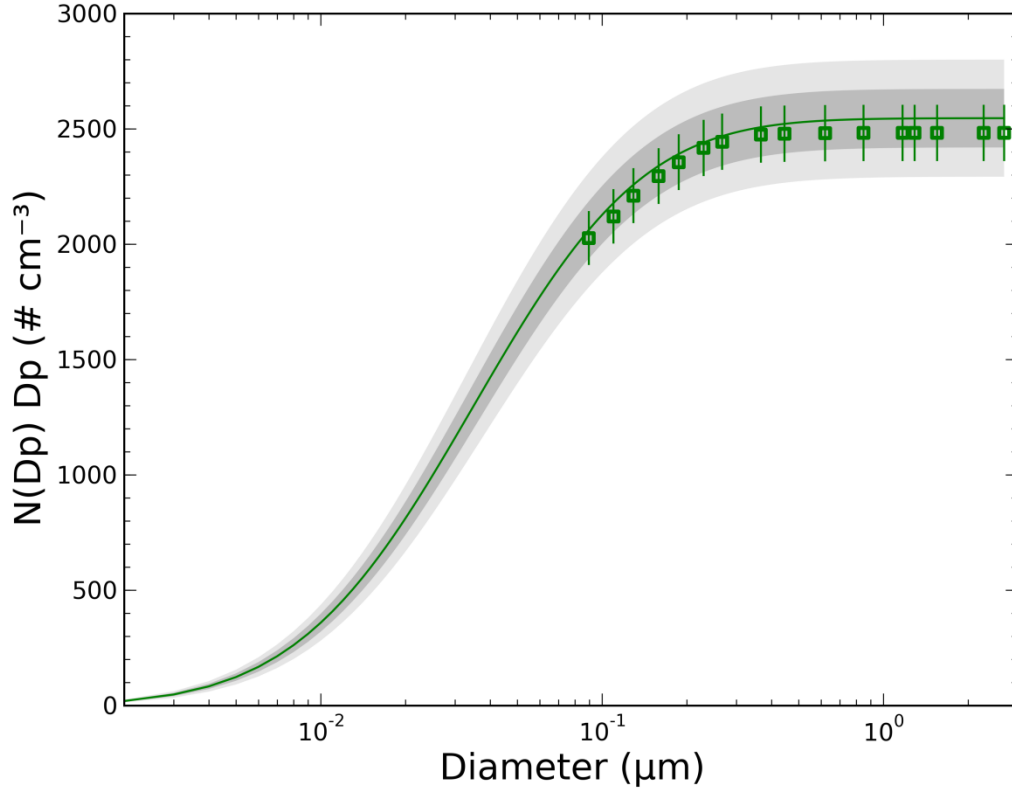


Figure 8: Cumulative size distribution representation of fitted and combined aerosol concentration data in Fig. 7.

After the best lognormal fit is constructed, predicted CCN amounts are calculated using D_c values calculated from the κ -Köhler theory and summing upwards on the number-size distribution function using the determined D_c points. It is shown from Fig. 7 that starting at 29 nm (D_c at 1.0 %) yields higher CCN concentration predictions (includes more area underneath the fit curves), than starting at 83 nm (D_c at 0.2 % SS). The resulting comparison between the CCN concentration prediction and measured CCN

values are shown in Fig. 9 for all the SS measurements made on 25 February 2009 case. Noticeably, progressing towards smaller particle size due to the crude extension of missing 0.01 to 0.9 μm range by one point measurement, fitting uncertainties get larger around these data points as depicted by the shaded ± 1 and ± 2 standard deviation coverage around the average fitting line in Fig. 7. This results in CCN over-predictions intensifying as SS increases.

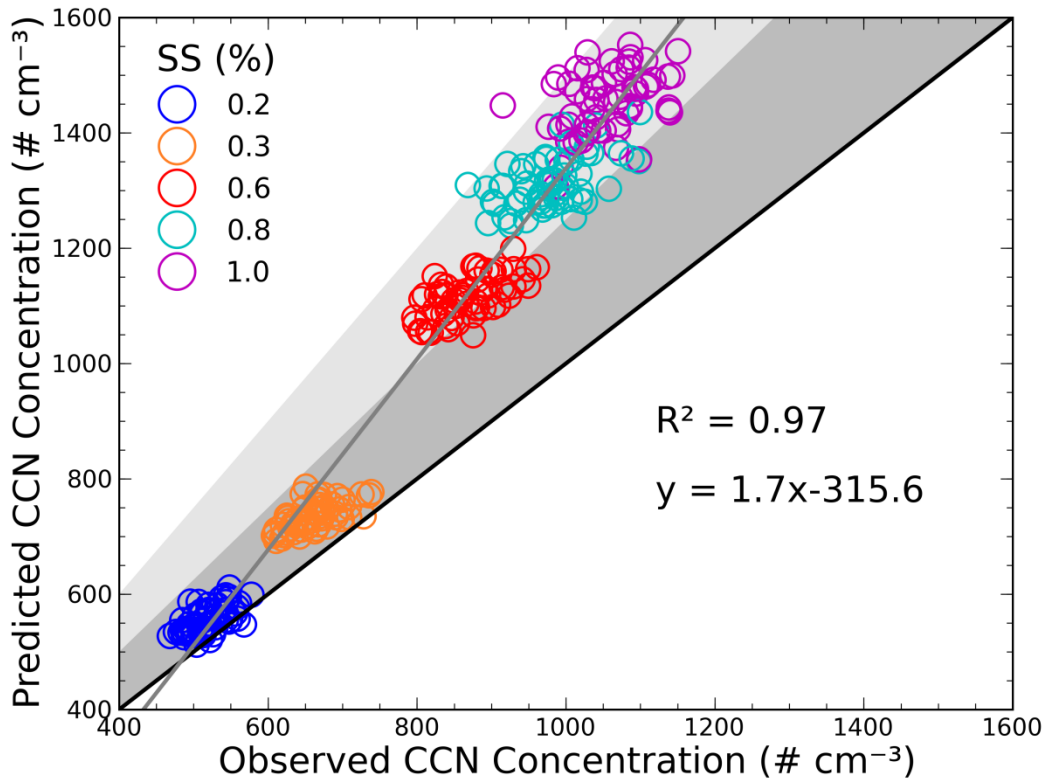


Figure 9: Measured and calculated CCN concentration comparison for the 25 February 2009 laboratory data. Each supersaturation (SS) measurement is grouped by different colors as given in the upper left located legend. The straight black line shows 1-to-1 correspondence, whereas the straight gray line shows the best linear fit on all plotted data with the equation given on the right along with the coefficient of determination result of the comparison. Dark and light shaded areas show 25% and 50% above the 1-to-1 line.

Table 3 lists fitting (gm, gsd) and CCN predicted / CCN measured ratio (CCN Ratio) statistics for all data used in the laboratory analysis. Here, a CCN ratio of less than one

represents that the CCN is overpredicted using the described approach. The results of these analyses are all computed with average and ± 1 standard deviation since one closure point section includes 10 second average of the whole study interval.

Table 3: Statistical results of the laboratory data analysis.

Data	SS (%)	CCN Ratio	R ²	CPC (# cm ⁻³)	PCASP (# cm ⁻³)	CCNC (# cm ⁻³)	GM (nm)	GSD
20090210 203159 (3000 seconds)	1.0	0.74 \pm 0.03	0.48	1300 \pm 67	280 \pm 11	616 \pm 29	41.4 \pm 1.6	2.90 \pm 0.04
20090224 2150589 (2000 seconds)	1.0	0.71 \pm 0.02	0.52	3014 \pm 152	581 \pm 21	1289 \pm 61	37.3 \pm 1.5	2.94 \pm 0.03
20090225 011651 (600 seconds)	1.0	0.68 \pm 0.02	0.14	4901 \pm 146	917 \pm 28	1979 \pm 57	36.4 \pm 1.2	2.93 \pm 0.02
20090225 034214 (600 seconds for each SS)	0.2	0.93 \pm 0.04	0.39	2454 \pm 124	469 \pm 19	519 \pm 25	36.7 \pm 1.8	2.97 \pm 0.03
	0.3	0.90 \pm 0.03	0.40	2412 \pm 115	453 \pm 15	661 \pm 32	36.1 \pm 1.6	2.97 \pm 0.02
	0.6	0.78 \pm 0.03	0.38	2400 \pm 114	454 \pm 16	868 \pm 42	36.2 \pm 1.7	2.97 \pm 0.03
	0.8	0.75 \pm 0.03	0.28	2457 \pm 113	465 \pm 17	979 \pm 50	36.2 \pm 1.6	2.98 \pm 0.02
	1.0	0.73 \pm 0.03	0.13	2482 \pm 122	456 \pm 16	1056 \pm 48	35.4 \pm 1.5	2.97 \pm 0.02

Field Data Analysis

Ground-based CCN Closure

Ground based data analysis is focused on the data obtained on 2 April 2009 in Riyadh, Saudi Arabia (Apr02, for brevity). An eighteen minute analysis interval was selected and divided into six sections per SS spectra availability as shown in Table 4. In the analysis range, a 0.27, 0.34, and 0.57 % SS cycle was repeated twice. Table 4 also lists the unimodal fitting parameters and summarizes the averaged aerosol and CCN measurements for each SS interval. Here, CPC and PCASP measurements are in good agreement in terms of magnitude comparison (i.e., higher N_t –both the average and variation corresponds to higher PCASP concentration, likewise low concentration correspondence is also apparent without any exception.) Similar comparison cannot be performed directly with the CCN measurements due to the SS dependence of reported

CCN values.

Analysis within the CCN measurement itself indicates that a slight over-counting in the first 0.27% SS segment comparing to the first 0.34% SS measurement. Twomey (1959) power-law based (in the form of $N = Cs^k$; where N being the CCN concentration, s is the supersaturation, C and k are the fitting parameters) CCN spectra fits reveal high CCN concentration measurements. C and k estimations, from Apr02 case, and five other ground-based CCN spectra measurements, are calculated along with associated curve-fit lines drawn for each case in Fig. 10. Based on the results annotated in Fig. 10, with the exception of high CCN load Apr05 and Apr13 cases, C and k values are in good agreement with Rogers and Yau's (1994) suggested classification of C and k range. They report $300 < C < 3000$ and $0.2 < k < 2.0$ ranges as optimum Twomey parameters of ground-based CCN measurements. CCN concentrations usually show variation depending on the time of the day, period of the year, proximity to the influencing sources (e.g., factory and urban area), and additional topographical features of the investigated area. Overall variation of k is in between 0.42-3.34 and 661.6 to 14960.6 for the C parameter. These listed reasons and high variation within the measured CCN data eliminate making generalized C and k parameter estimates for the study of region.

Table 4: Part 1 of Apr02 ground data statistics and analysis results.

Analysis Interval (SFM / HH:MM:SS)	SS (%)	CPC (# cm⁻³)	PCASP (# cm⁻³)	CCNC (# cm⁻³)	GM (nm)	GSD
43440 – 43620 (12:04:00 – 12:07:00)	0.27	18652 ± 2124	679 ± 30	1001 ± 171	21.4 ± 0.2	2.42 ± 0.03
43620 – 43800 (12:07:00 – 12:10:00)	0.34	16981 ± 1084	628 ± 19	994 ± 42	21.3 ± 0.1	2.42 ± 0.01
43800 – 43980 (12:10:00 – 12:13:00)	0.57	17970 ± 2345	662 ± 61	1534 ± 207	21.4 ± 0.1	2.42 ± 0.01
43980 – 44160 (12:13:00-12:16:00)	0.27	18253 ± 2821	671 ± 67	848 ± 353	21.4 ± 0.1	2.42 ± 0.02
44160 – 44340 (12:16:00 – 12:19:00)	0.34	15192 ± 405	594 ± 8	872 ± 55	21.5 ± 0.1	2.44 ± 0.01
44340 – 44520 (12:19:00 – 12:22:00)	0.57	17438 ± 639	636 ± 16	1466 ± 170	21.3 ± 0.1	2.42 ± 0.01

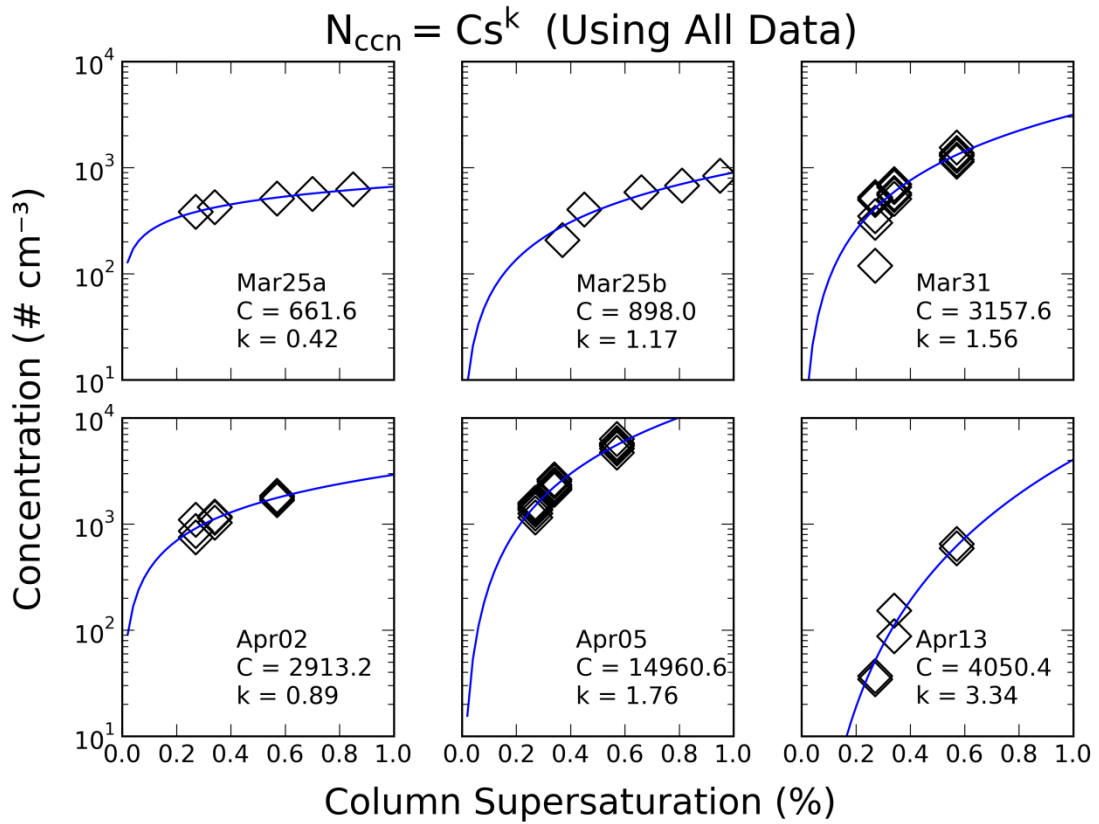


Figure 10: Twomey power-law based CCN concentration estimations and curve-fits constructed based on the most optimum C and k parameters estimated from ground-based CCN concentration spectra. This figure includes the ground CCN closure case (Apr02 – bottom left panel) and five other cases.

CCN closure is performed by varying κ from 0.6 to 0.1 low hygroscopic values with 0.1 decrements and estimating the optimum κ range. This establishes the most optimum agreement in between predicted and CCN concentration and at the same time, determines the hygroscopicity of the measured aerosol. Table 5 lists the CCN concentration ratios (CCN measured / CCN predicted), R^2 values, and D_c values for each SS for three different values of κ . It is evident that D_c is inversely related to κ and SS, as explained earlier when discussing Fig. 3.

In considering R^2 , low R^2 values for 0.34% SS analysis interval are possibly indicative of outliers in the data points, which is worsening the correlations of predicted

Table 5: Part 2 of Apr02 ground data statistics and analysis results.

SS (%)	$\kappa = 0.6$			$\kappa = 0.4$			$\kappa = 0.2$		
	CCN Ratio	R ²	D _c (nm)	CCN Ratio	R ²	D _c (nm)	CCN Ratio	R ²	D _c (nm)
0.27	0.53 ± 0.15	0.99	67	0.71 ± 0.19	0.98	77	1.21 ± 0.30	0.97	97
0.34	0.45 ± 0.03	0.07	58	0.58 ± 0.04	0.06	66	0.94 ± 0.05	0.06	83
0.57	0.37 ± 0.03	0.69	41	0.45 ± 0.04	0.69	47	0.67 ± 0.06	0.70	59
0.27	0.51 ± 0.13	0.99	67	0.68 ± 0.17	0.99	77	1.14 ± 0.29	0.99	97
0.34	0.43 ± 0.03	0.01	58	0.55 ± 0.04	0.02	66	0.88 ± 0.06	0.04	83
0.57	0.36 ± 0.04	0.46	41	0.45 ± 0.05	0.48	47	0.67 ± 0.07	0.52	59
Overall →	0.42 ± 0.09	0.80		0.54 ± 0.12	0.80		0.86 ± 0.22	0.79	

and observed CCN concentrations. CCN ratio analysis shows over-predictions in the given $\kappa = 0.6 - 0.2$ range with the exception of 0.27% SS intervals (ratios over 1 means under-estimated prediction of CCN concentration.) Additionally, lower 0.27 and 0.34% SS associated ratios give a better agreement in the $\kappa = 0.4 - 0.2$ range as opposed to the 0.57% SS analysis interval. The final analysis in the ground CCN closure shows overall variation of CCN ratio as illustrated in Fig. 11 with box-and-whiskers plots. Fig. 11 shows the variation of CCN measured / CCN predicted ratios for the full set of κ values.

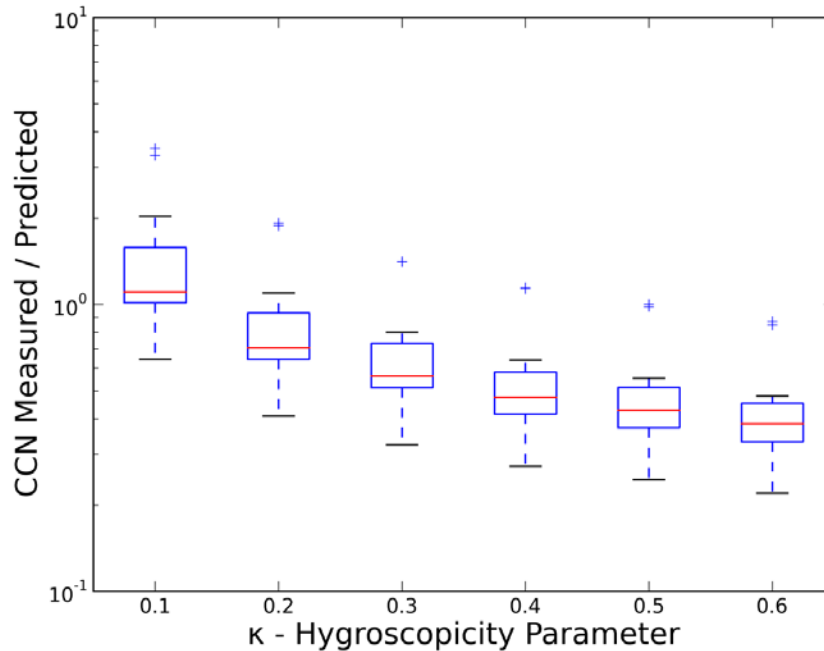


Figure 11: Variation of CCN ratio over the range of the six different κ assumptions. In the box-and whiskers plots, red lines show the median of ratios, lower and higher ends of

the boxes show 25% and 75% percentile of the data, whiskers denote the range of the data, and flier points (blue plus signs) show outliers.

Airborne CCN Closure

The cloud-base time intervals were determined from front-facing video camera recordings and verified by measured atmospheric data (e.g., ambient and dew point temperatures and liquid water content amount per interval). Cloud-base temperatures of all the cases, with the exception of Apr09 case, were warmer than freezing. Table 6 presents the analyzed cases, selected intervals, aerosol and CCN concentrations, and the unimodal lognormal function fitting statistics obtained from the PCASP and CPC combined size spectra.

Table 6: Part 1 of the airborne data statistics and analysis results. Note that all CCN concentrations are reported at 0.61% SS setting.

Data ID	Cloud Base Start-Stop (SFM / HH:MM:SS)	Closure (second)	CPC (# cm⁻³)	PCASP (# cm⁻³)	CCNC (# cm⁻³)	GM (nm)	GSD
090402 131020 (Apr02a, Apr02b)	49045 - 49445 (13:37:25 - 13:44:05)	400	866 ± 231 635 405	284 ± 37	404 ± 42	77.0±20.3 114.1±32.3 163.4±37.3	3.25±0.37 2.63±0.53 1.90±0.65
	55410 - 55600 (15:23:40 - 15:26:40)	180	769 ± 183 587 404	224 ± 41	298 ± 40	66.4±15.2 90.1±21.4 129.7±33.6	2.98±0.31 2.56±0.32 2.03±0.38
090406 130109 (Apr06)	47580 - 48080 (13:13:00 - 13:21:20)	500	1576 ± 511 1065 554	250 ± 30	432 ± 42	37.0±7.1 63.2±22.4 126.9±54.4	3.38±0.16 3.10±0.37 2.11±0.81
090408 123026 (Apr08)	48240 - 48490 (13:24:00 - 13:28:10)	250	1309 ± 100 1209 1108	414 ± 31	563 ± 50	72.2±5.4 79.0±5.9 86.7±6.5	2.95±0.17 2.82±0.17 2.68±0.16
090409 123225 (Apr09)	51285 - 51495 (14:14:45 - 14:18:15)	210	806 ± 86 720 634	274 ± 58	297 ± 52	79.5±9.1 85.6±8.6 92.7±7.8	2.03±0.39 1.96±0.35 1.86±0.34
090412 115713 (Apr12)	48395 - 48685 (13:26:35 - 13:31:25)	290	4844 ± 2336 2508 171	823 ± 251	820 ± 272	59.7±16.7 71.9±30.8 69.0±45.9	2.12±0.55 1.67±0.35 1.45±0.28

The same field calibrated PCASP channel size limits (0.112, 0.136, 0.161, 0.197, 0.232, 0.285, 0.381, 0.658, 0.933, 1.367, 2.194, 2.680, 2.893, 3.481, 4.501, 5.413) were used for the airborne measurements as for the ground-based measurements; however, the

size boundaries are a lot different from the boundaries used for the laboratory measurements, since a different PCASP was used during the Spring 2009 field project. The selected cloud-base intervals contain only 0.61% SS set CCN measurements; therefore, only one CCN concentration value is reported for each interval (in average ± 1 standard deviation CCN measurement form).

As in the ground-based CCN closure analysis steps, airborne closure was performed by following the κ varied (0.6 – 0.1) scheme. Table 7 reports the results of each cloud-base CCN closure for each κ and corresponding D_c point calculated at 0.61% SS in κ -Köhler theory. In this section, previously used CCN ratio (measured CCN / predicted CCN concentration ratio) based closure assessment was replaced by the more robust relative error indicator (Rel. Err. (%) in Table 7). Here, the relative error of CCN over / under estimation is defined as:

$$Relative\ Error\ (\%) = \frac{CCN\ predicted - CCN\ measured}{CCN\ measured} \times 100 \quad (6)$$

In the relative error representation, positive values mean over estimation, while negative values represent under estimation of observed CCN concentration compared to the unimodal fit based prediction approach. Smaller relative errors mean higher closure agreements, simply making the predictions in good agreement with measurements. The reason that the error is reported in average \pm one standard deviation % form is because, each closure case contains 10 seconds averaged analysis points, therefore giving a sequence based comparison rather than a scalar comparison.

The other important difference is that the effect of the CPC measured N_t on the CCN closure was assessed by using the actual average total per interval, one and two standard deviations below the average N_t . This explains the reason of having three rows of the

CPC statistics and three gm and gsd rows for each case in Table 6, also having three Rel. Err. And R^2 rows per κ in Table 7. Six case combined, overall analysis results are listed in Table 8 for the average N_t , one and two standard deviations below the average N_t , and corresponding $\kappa=0.6$ and $\kappa=0.1$ analysis.

Table 7: Part 2 of the airborne data statistics and analysis results. Note that all CCN closure calculations are performed at 0.61% SS setting.

κ	D_c (nm)	Apr02a		Apr02b		Apr06	
		Rel. Err. (%)	R^2	Rel. Err. (%)	R^2	Rel. Err. (%)	R^2
0.6	39	48 ± 14	0.51	72 ± 12	0.75	68 ± 25	0.20
		27 ± 15	0.55	53 ± 15	0.63	44 ± 26	0.20
		-12 ± 28	0.47	19 ± 24	0.38	-11 ± 52	0.15
0.5	42	43 ± 13	0.49	66 ± 11	0.78	59 ± 23	0.21
		25 ± 14	0.55	49 ± 13	0.67	39 ± 23	0.21
		-12 ± 26	0.47	17 ± 22	0.41	-13 ± 50	0.16
0.4	45	39 ± 13	0.47	60 ± 11	0.80	51 ± 21	0.22
		22 ± 13	0.55	45 ± 12	0.71	33 ± 21	0.22
		-13 ± 25	0.48	15 ± 20	0.44	-15 ± 47	0.16
0.3	49	34 ± 13	0.44	53 ± 10	0.72	41 ± 18	0.23
		19 ± 12	0.54	39 ± 10	0.75	27 ± 19	0.23
		-14 ± 24	0.48	13 ± 18	0.48	-17 ± 44	0.17
0.2	56	25 ± 12	0.39	40 ± 8	0.86	26 ± 15	0.25
		13 ± 11	0.52	30 ± 8	0.82	16 ± 15	0.25
		-16 ± 22	0.49	9 ± 15	0.57	-22 ± 39	0.18
0.1	71	8 ± 12	0.30	18 ± 7	0.89	1 ± 11	0.27
		2 ± 10	0.44	12 ± 6	0.89	-3 ± 11	0.28
		-20 ± 17	0.51	-1 ± 9	0.76	-30 ± 32	0.20
κ	D_c (nm)	Apr08		Apr09		Apr12	
		Rel. Err. (%)	R^2	Rel. Err. (%)	R^2	Rel. Err. (%)	R^2
0.6	39	67 ± 11	0.49	134 ± 35	0.39	290 ± 70	0.75
		62 ± 10	0.55	116 ± 28	0.52	120 ± 155	0.81
		56 ± 9	0.62	97 ± 23	0.63	-9 ± 116	0.68
0.5	42	61 ± 11	0.47	128 ± 34	0.37	273 ± 66	0.75
		57 ± 10	0.53	111 ± 28	0.49	114 ± 147	0.81
		51 ± 9	0.60	93 ± 23	0.60	-8 ± 111	0.68
0.4	45	56 ± 11	0.45	121 ± 33	0.36	257 ± 63	0.74
		52 ± 10	0.51	106 ± 28	0.47	106 ± 140	0.81
		47 ± 9	0.58	90 ± 23	0.57	-9 ± 107	0.69
0.3	49	49 ± 10	0.23	112 ± 32	0.36	235 ± 59	0.74
		46 ± 10	0.49	99 ± 27	0.45	97 ± 131	0.81
		42 ± 9	0.56	84 ± 23	0.54	-11 ± 102	0.69
0.2	56	38 ± 10	0.41	95 ± 29	0.37	199 ± 54	0.75
		36 ± 9	0.46	85 ± 26	0.44	79 ± 116	0.81
		32 ± 8	0.52	74 ± 22	0.51	-16 ± 94	0.70
0.1	71	18 ± 9	0.38	59 ± 22	0.44	130 ± 46	0.76
		17 ± 8	0.42	54 ± 21	0.48	45 ± 89	0.81
		15 ± 8	0.47	48 ± 20	0.50	-27 ± 78	0.73

Table 8: Overall statistical results of the airborne CCN closure.

Overall Results	<CPC>		<CPC> - 1 STDDEV		<CPC> - 2 STDDEV	
	$\kappa = 0.6$	$\kappa = 0.1$	$\kappa = 0.6$	$\kappa = 0.1$	$\kappa = 0.6$	$\kappa = 0.1$
Rel. Err. (%)	107 ± 90	34 ± 50	64 ± 74	17 ± 43	14 ± 8	-10 ± 45
R^2	0.79	0.79	0.77	0.80	0.50	0.55
Slope	4.27	2.32	3.72	2.19	2.01	1.43
Intercept	-953	-425	-915	-453	-392	-241

Figure 12 shows the instrumental data statistics that are listed in Table 6, graphically via box-and-whiskers plots. For each instrument, boxes are filled with a different color as specified by the annotated text located in the middle of the panels. Apr06 and Apr12 cases instrumental data temporal changes are shown in Fig. 13 for a total of 290 seconds interval. Note that, in both Figs. 11 and 12, the CPC measurements used are the actual reported N_t .

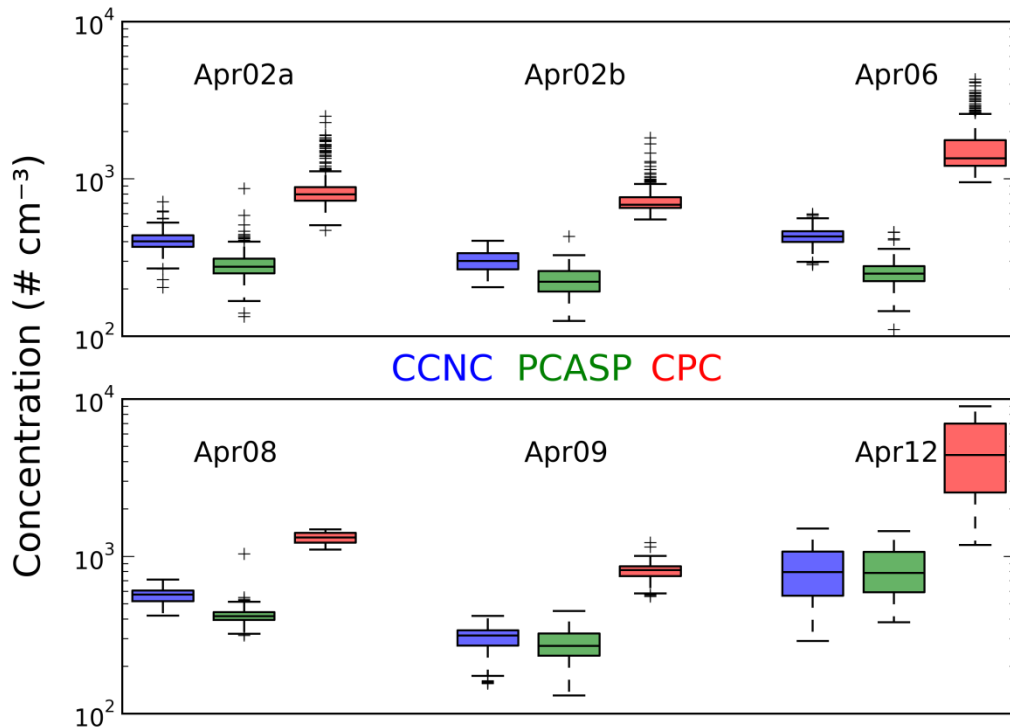


Figure 12: Box-and-whiskers plot representation of the CCNC, PCASP and CPC data for all the cases that are given in Table 6.

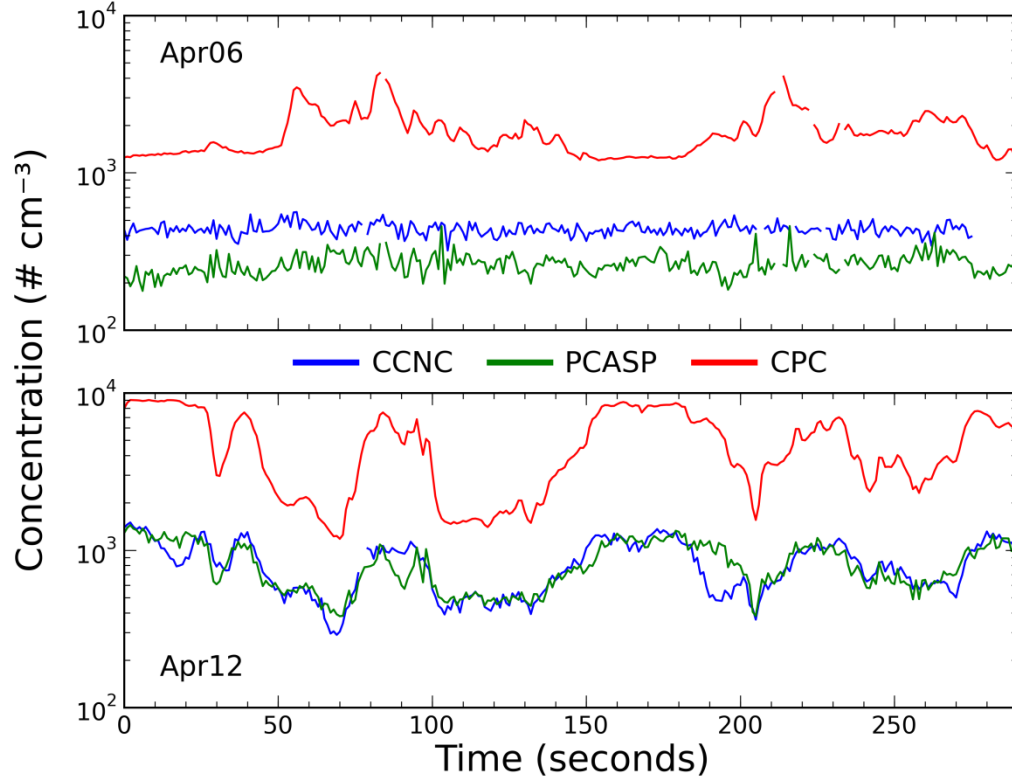


Figure 13: Time-series representation of the CCNC, PCASP and CPC data for the time-intervals specified in Table 6, for the upper panel shown Apr06 and the lower panel Apr12 cases.

Discussions

In the laboratory section of the data analysis, the CCN closure showed 7 to 38% over prediction of the CCN concentration, based on the PCASP and CPC combined particle size spectra fitting in the increasing 0.2 to 1.0% SS direction using the $\kappa = 0.6$ assumption of the measured AS aerosol. The closure approach was modified in field data analysis section to assess the hygroscopicity of the measured particles via κ varying CCN predictions. In the single day ground-base case, the closure was achieved between $\kappa = 0.4$ and $\kappa = 0.2$ for 0.27% SS intervals. 0.34% SS closure can be achieved in $\kappa = 0.2$ and 0.1, whereas 0.57% SS closure agreement requires the $\kappa < 0.1$ assumption of the aerosol.

In the airborne data analysis section, the closure tests expanded to determine the

effect of the CPC measured N_t in the unimodal distribution assumption of the measured aerosol. Closure results are case dependent and highly variable based on the varied peak aerosol concentration. Within 10% uncertainty limit, the closure was achieved only on Apr02a and Apr06 cases when the actual N_t used for $\kappa < 0.2$ assumption. Within 20% uncertainty limit, again only Apr02a and Apr06 cases result with a reasonable closure agreement using one standard deviation below the actual N_t , for $\kappa < 0.3$ and $\kappa < 0.2$, respectively. For two standard deviations below N_t tests, meaningful comparisons are not possible since gm of the first three cases shift to the PCASP measurement range, resulting with systematic under-prediction of CCN for each $\kappa = 0.6$ assumption. Also important in the uncertainty analysis, some cases have higher N_t variation which are causing unrealistic deviations for the selected κ values (e.g., Apr12).

Apr12 case was expected to give the best closure agreement due to the high shape correlation of the measured PCASP and CPC aerosol data as shown in the lower panel of the Fig. 13. However, the unimodal fitting technique and 10 seconds averaging based CCN predictions fail to capture the measured CCN concentration. The failure is mostly attributed to the high variation of the CPC data ($10^3 - 10^4 \text{ # cm}^{-3}$) and the fact that 10 seconds averaging of the analyzed data cannot represent the high step change in the PCASP and CPC data. In contrast to Apr12, relatively less varying Apr06 case (the top panel in Fig. 13) yields reasonable results for the $\kappa < 0.2$, except the two standard deviations below the actual N_t comparisons.

Estimation of the two log-normal fitting parameters (gm and gsd) are heavily influenced by including / excluding first two channels of the PCASP data which the reliability of those is object to question. The geometric mean diameter (gm) is controlled

by the CPC / PCASP data ratio. When this ratio is large, gm estimations become lower. Similarly, lower CPC / PCASP ratios yield higher gm estimates. There is an inverse relation between gm and gsd values. That is when gm is larger, in order to compensate this shift, gsd values are decreased, leading to narrow shaped curve fits. This means clearly that in the case of erroneous modal representation of the aerosol spectra, gm and gsd values are only valid within statistical perspective, but cannot be considered meaningful or well-representative of the data from the physical reasoning point of view.

Conclusions

The following points are concluded in this CCN closure analysis:

1. For the purpose of CCN prediction, PCASP and CPC combined data based unimodal lognormal fitting function assumption does not perform well for 0.3% and above SS range CCN comparisons.
2. Fit parameters gm and gsd are controlled by the CPC and PCASP concentration ratios, irrespective of the actual PCASP size distribution due to the unimodal log-normal fitting assumption.
3. Closure agreements are highly dependent on the number of the data points and data range over which the log-normal function is estimated.

The first and second conclusions could be improved by having extended high resolution size spectra of aerosol data down to at least 40 nm to achieve reasonable agreements for 0.6% and below SS based closures. Alternatively, having lower SS CCN measurements improves the closure agreement since D_c falls near or within the PCASP measurements, hence yielding more reliably predicted CCN concentrations. The third conclusion emphasizes the importance of the size calibration of the PCASP. Analyses

that were conducted with not-well calibrated PCASP data showed substantially different CCN closure results.

Although it is not feasible to determine the exact aerosol hygroscopicity of airborne data within $k < 0.6$ space, due to the relatively high set SS measurements of the CCN data, ground-based 0.27% range predictions indicate the κ values of the particles could be within 0.2 and 0.4 range.

CHAPTER IV

AEROSOL – CLOUD DROPLET NUMBER CONCENTRATION (CDNC) CLOSURE

Introduction

One of the key uncertainty sources of aerosol-cloud interactions (that is the predictability of cloud droplet number concentration (CDNC or N_d)) is studied in this section using the convective 2 April 2009 (hereafter, Apr02 for brevity) cloud-base and in-cloud measurements. As noted by Fountoukis et al. (2007) the ultimate goal of this test is to compare and contrast the predicted N_d against in-situ measurements and determine the sources of discrepancies in closure. The main ingredients of the cloud model that is going to perform the calculations are below cloud updraft velocities, cloud-base aerosol size and concentration, and assumptions about the chemical composition of the PCASP and CCNC sampled aerosol. Within the scope of this study, the variation of aerosol chemical composition assumption and cloud-base measured average/actual velocities are evaluated first, then the effects of PCASP aerosol concentration variation is assessed. The following section provides the basic theory behind the cloud parcel model. Details about the model setup and testing of parameter sensitivities are described in the methodology section. The next section discusses the possible reasons of the closure discrepancies and the final remarks are presented in the final conclusion section.

Theory

The proposed aerosol / cloud droplet number concentration closure study is

performed by employing a 1D binned cloud parcel model. The model is based on a closed / adiabatic assumption under constant vertical velocity. Description of the original model is given in Appendix A of Snider et al. (2003). The thermodynamic energy, water vapor mixing ratio, and condensational droplet growth equations are the key computational steps in the model. Temperature evolution of the parcel is controlled by the thermodynamic energy equation which is given by Eq. 6.

$$\Delta T = - \frac{(1+r_v+r_l)gw\Delta t+l_v\Delta r_v}{c_p} \quad (6)$$

Here, ΔT is the temperature increment per model time step, r_v and r_l are the mixing ratios of vapor and liquid, g is the gravitational acceleration, w is the updraft velocity, l_v is the latent heat vaporization, Δr_v is the step-increment in the vapor mixing ratio and c_p is the specific heat capacity at constant pressure. The water vapor mixing ratio is implemented as:

$$\Delta r_v = r_{l,pre} + \left(\frac{\pi}{6}\right) \sum n_j (1 - x_j) \rho_j (D_j^3 - D_{jin}^3) \quad (7)$$

where v is the parcel volume, $r_{l,pre}$ is the liquid water mixing ratio calculated at the previous time step, n_j is the particle concentration in bin j , x_j is the salt weight fraction in the solution, ρ_j is the solution density, D_j and D_{jin} are the sizes corresponding to the complete particle and its insoluble part.

Droplet growth equation is based on the equation developed by Zou and Fukuta (1999) and is given as:

$$D_k = \frac{\Delta t(S-S_k)\Psi_k}{D_{k,pre}} + D_{k,pre} \quad (8)$$

where $D_{k,pre}$ is the particle diameter calculated from previous time step, S and S_k are the ambient and particle saturation ratios, respectively, and Ψ_k is a coefficient varying with

particle size, pressure, temperature and the condensational-diffusional accommodation coefficients. Within the parcel model, thermodynamic energy and mixing ratio equation loops evolve in 0.2 seconds per calculation step, whereas the condensational growth equation evolves at 0.02 seconds per step calculation.

Methodology

The first step in the parcel model based analysis is to determine cloud-base interval from which the model is initialized and the next in-cloud pass interval to use in the comparison of the observed and predicted N_d . As in the CCN closure analysis, the cloud-base interval was determined by front-facing camera recordings, and the in-cloud pass is determined from the altitude profile of the Apr02 flight and the exact time interval determined from liquid water content (LWC) and N_d observations. Figures 14 and 15 give the time-series measurements during the Apr02 flight when sampling below and just above cloud base. The below cloud based measurements occasionally encounter cloud regions (such as just after 550 seconds in Figure 15); therefore for the analysis presented here, all below cloud based measurements are filtered to remove time periods with FSSP concentrations above 50 \# cm^{-3} .

The PCASP measured aerosol size spectra and CCNC measurements (Fig. 16 bottom panels) provide data for initialization of the model. The model uses κ -Köhler theory for saturation ratio and critical activation diameter estimations. Aerosol initialization is grouped into two main particle modes: i) Accumulation/coarse, ii) Aitken. The accumulation/coarse mode, number concentration and the dry particle radii are obtained from the PCASP aerosol measurements and mid-point channel limits, respectively. Given the dry particle radii and applying the κ -Köhler theory critical wet particle radii are

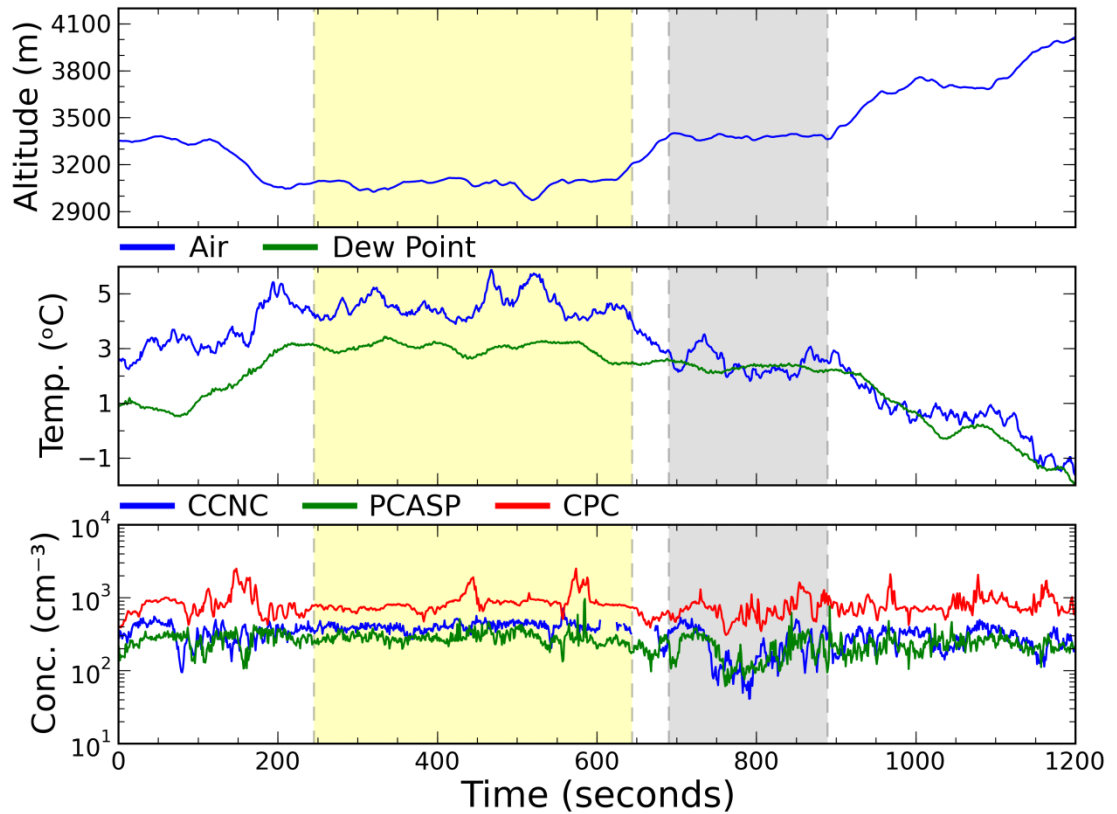


Figure 14: Twenty minutes time-series from 13:33:20 – 13:53:20 UTC on the 02 April 2009 aircraft flight. The yellow and gray shaded regions are the cloud-base and in-cloud sampling periods, respectively. The top panel shows the pressure altitude. The middle panel shows the ambient air temperature (blue line) and the dew point temperature (green line). The bottom panel shows the 0.61% supersaturation Cloud Condensation Nuclei (CCN) concentration (blue line) measured with a Droplet Measurements Technology counter, the total (approximately 0.1 to 5.4 μm diameter) optical aerosol concentration (green line) measured by a model 100 Passive Cavity Aerosol Spectrometer Probe (PCASP), and the Condensation Nuclei (particles larger 10 nm in diameter) concentration measured by a TSI Condensation Particle Counter model 3772.

calculated. Here, it is assumed that the PCASP measured particle size spectra only composed of dry particles as noted in Liu et al. (1992). Corresponding critical activation supersaturation is also calculated to determine if a particle is activated or not in the parcel model simulation. Using the EG/G hygrometer derived maximum cloud-base relative humidity (RH=95%), initial wet particle radii are estimated. Similar estimations are made for the Aitken mode particles except that the construction of the Aitken mode is

based on the power-law fit that is estimated on one point (0.61% SS) measurement. Since there is a single measurement point, the k value from $N = Cs^k$ in the two unknowns equation, is surrogated by the same day ground CCN spectra k value as was constructed in the CCN closure chapter (Fig. 10). This assumes that the shape of the CCN supersaturation spectrum is similar between the surface and cloud base measurements.

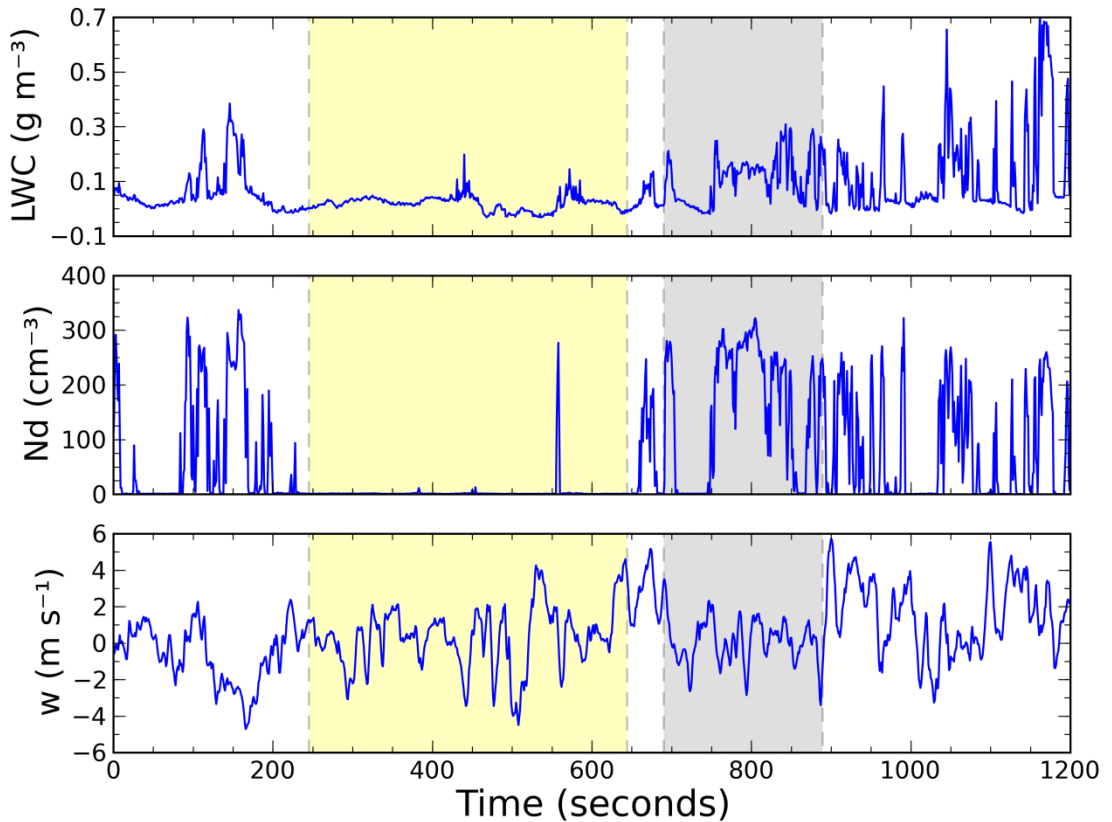


Figure 15: Similar to the Fig. 14, except the top panel shows the DMT Hotwire liquid water content (LWC), the middle panel shows SPP-100 model FSSP cloud droplet concentration, and the bottom panel shows the Sky Avionics Ball variometer vertical velocity.

As it is seen from Fig. 17, larger particles require less supersaturation to become activated. However, Aitken mode particles require high SS values to become cloud particles. As it will be shown later in Fig. 20, even the maximum observed updraft velocity is not sufficient to activate the smallest Aitken mode particles, solely based on

the condensational growth. Accumulation/coarse mode activation spectra assuming $\kappa = 0.1$ and 1.0 hygroscopicity are shown in Fig. 17. Effects of the activation degree can be clearly seen on the lower end of the SS axis as the critical activation SS shifts to higher supersaturation values as κ decreases.

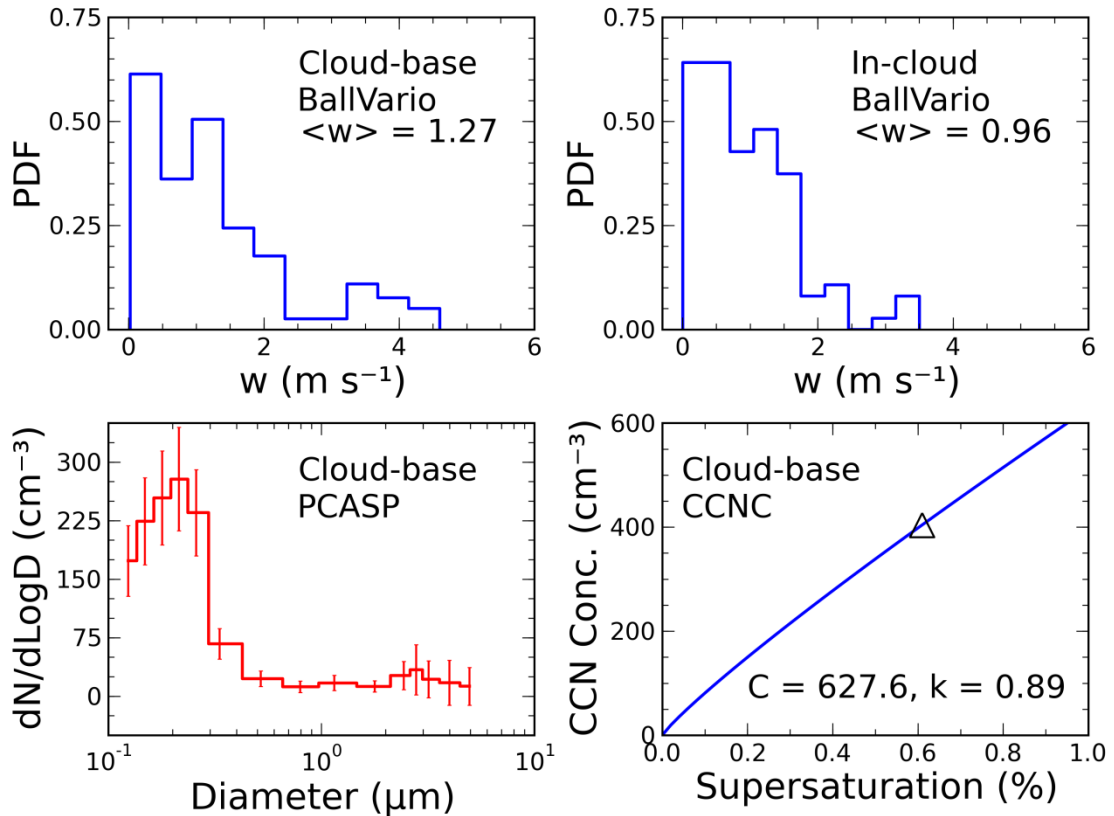


Figure 16: The top panels show normalized histograms (binned in 10 intervals) of the cloud-base and in-cloud updrafts (for $w > 0$). Average updrafts for the presented section are also noted with $\langle w \rangle$ notation. The bottom-left panel shows cloud-base normalized average PCASP aerosol spectra. Normalized ± 1 standard deviation aerosol spectra are overlaid on the average step plot using vertical lines. The bottom-right panel shows supersaturation spectrum based on the 0.61% supersaturation measurement and the k parameter value obtained from pre-flight surface CCN spectrum measurements.

The observed minimum and maximum cloud base updraft velocities are between 0 and 4.6 m s^{-1} with an average value of 1.3 m s^{-1} . For each $\kappa = 0.1$ and $\kappa = 1.0$, the model is run for the average w and 10 different steps of the actual w range. For the average w

value, the parcel model is executed only once and for the latter case the model is run 10 times producing 10 corresponding activated N_d for each w in the binned range. Throughout the model execution, w is constant at all time intervals and parcels are lifted from the 95% RH level (693.7 hPa) up to 685.1 hPa (approximately 203 meters above the initialization point) before the model execution is finished. The final predicted droplet estimation is made based on the interpolation of the model produced N_d values and the interpolation of these in the w range that is obtained from the cloud-base measurements.

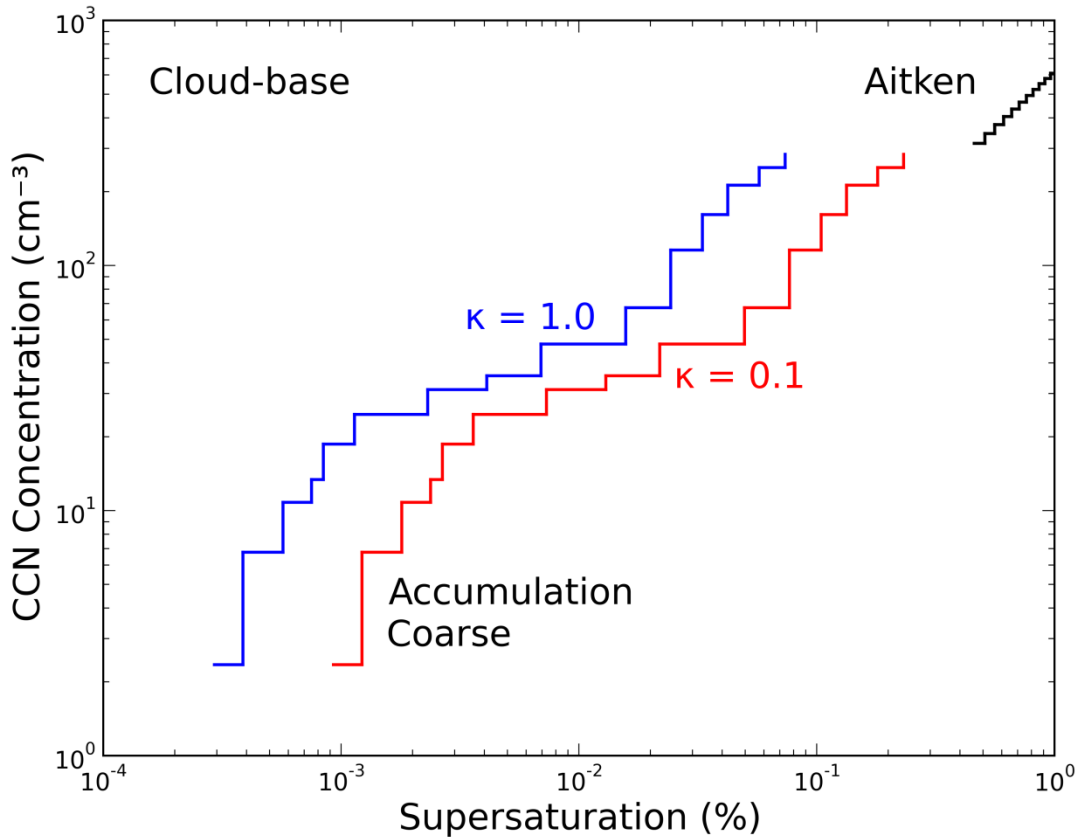


Figure 17: Activation spectra of the accumulation-coarse and Aitken mode aerosol. The accumulation-coarse mode spectra are based on the average cloud-base PCASP aerosol measurements from the Apr02 flight and $\kappa = 0.1$ and 1.0 hygroscopicity assumption as drawn by red and blue colors, respectively. Aitken mode spectra is constructed from the power-law fit as described in the methodology section.

Results and Discussion

The two key parameters that determine the final predicted N_d are CCN spectra and cloud updraft velocity. The former is constructed by converting the PCASP measured aerosol size distribution using the κ -Köhler equations to obtain accumulation and aiten mode aerosols and combining these with the actual airborne CCN measurements. Since size-segregated chemical composition measurements were not made, the same hygroscopic growth is assumed the same for all size bins. In this study two κ values are used for testing chemical composition assumption of measured aerosol.

Test simulations were performed to investigate the SS profiles within the parcel model. Fig. 18 demonstrates one such attempt under two different κ and two w

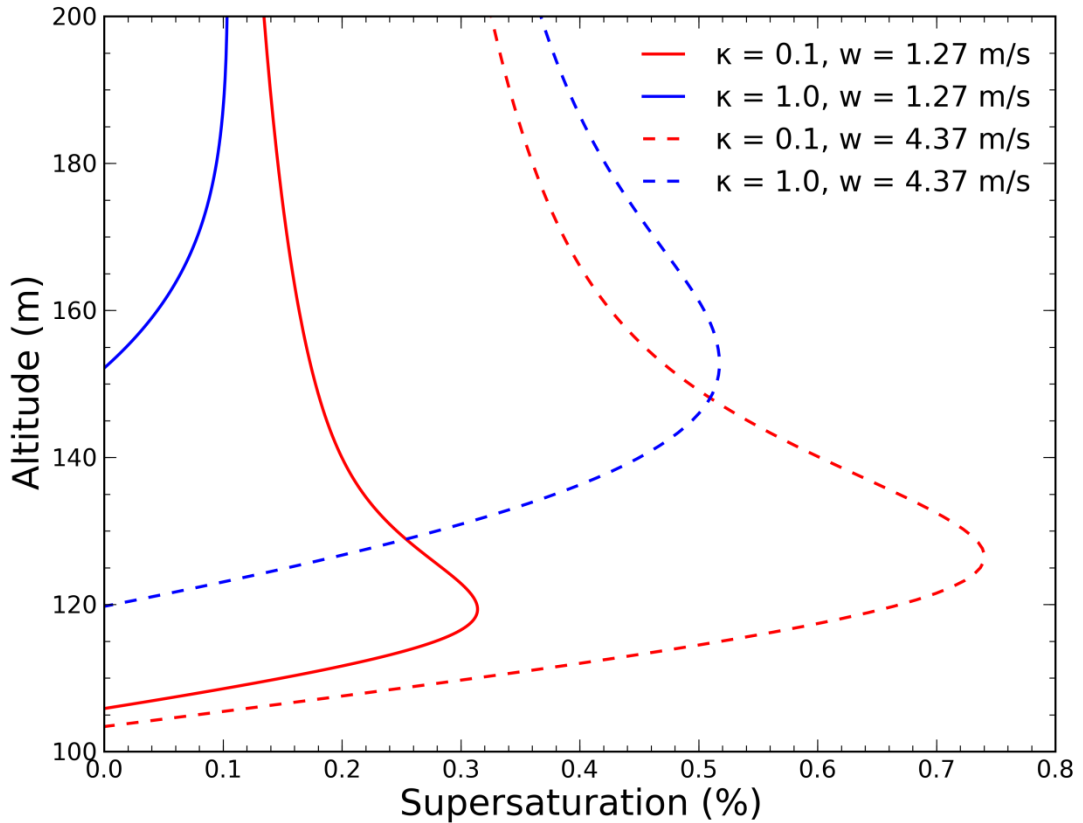


Figure 18: Vertical SS profiles as experienced in the parcel model with the four distinct initialization conditions noted in the upper-right corner of the figure.

initialization settings. For all cases shown in the Fig. 18 maximum supersaturations are reached above the first half (above 100 m) of the parcel model simulation. Under $\kappa = 1.0$ and $w = 1.27 \text{ m s}^{-1}$ setting the parcel experiences the lowest SS, while for the low hygroscopic / maximum w initialization condition the parcel can experience maximum SS up to 0.74% level.

Cloud updraft velocity is directly proportional to in-cloud supersaturation which determines how much of the aerosol is activated within cloud and how much of this activated aerosol is going to continue growing to become cloud droplets by condensational growth process at the expense of the available ambient supersaturation. In the current configuration of the model w is represented by a discretized range (w -PDF hereafter for the brevity) as described in the previous section. In addition, simulations using the mean updraft velocity (w -mean) are performed since Fountoukis et al. (2007) report that using average updraft velocity is sufficient to calculate droplet concentrations to achieve a successful closure. The model predicted and observed N_d comparisons are made based on the plots shown in Fig. 19. In the figure, normalized histograms of observed ($N_d > 50 \text{ cm}^{-3}$) and the model predicted N_d are overlaid for each model initialization setting as noted on the upper-left corners of the plots. The comparison is focused on two different κ values and using the average w and w -PDF based initializations. This comparison method is particularly important in assessing the contribution of the vertical velocity distribution for cloud droplet activation. Independent of the κ setting, average w based parcel model prediction of N_d (cases a and c) results in 15.7% under-prediction of the observed N_d . When the full w range is employed, $\kappa = 0.1$ run (case b) yields 9.8% over-prediction, while $\kappa = 1.0$ (case d) run results with 2%

under-prediction of cloud droplets.

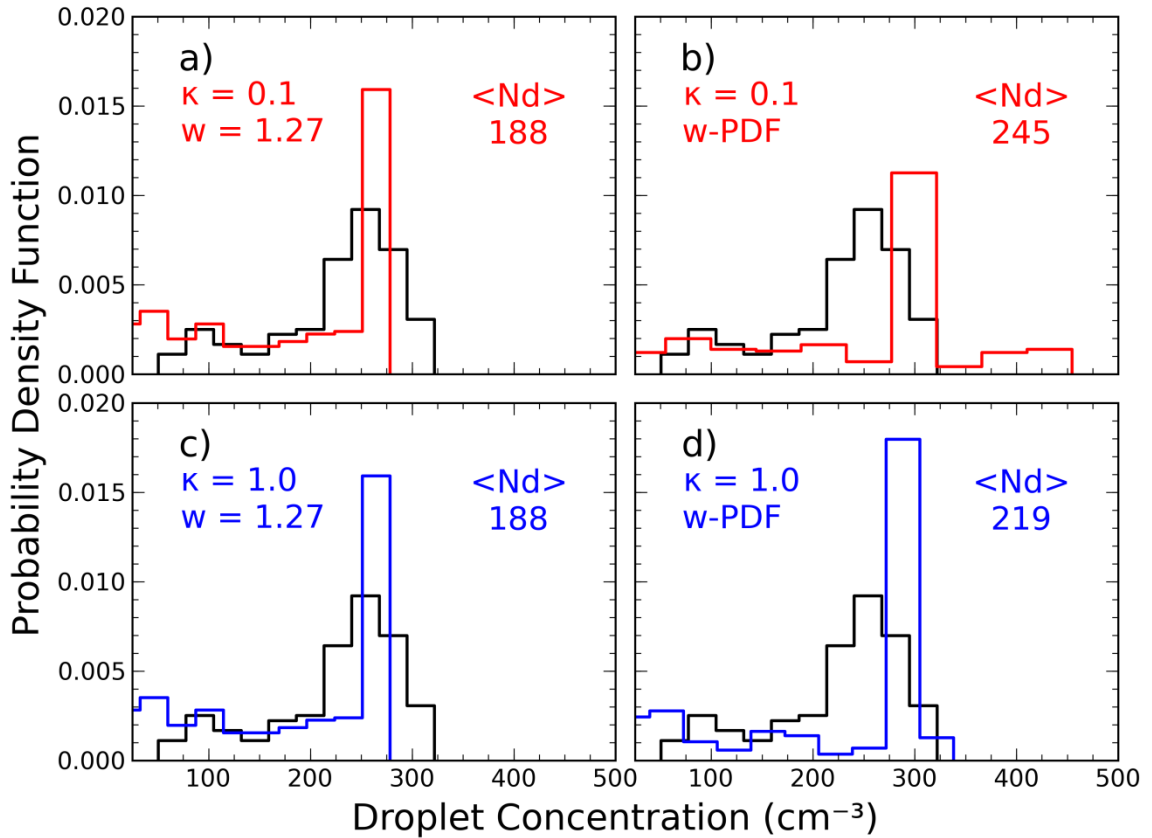


Figure 19: Comparisons of the parcel model predicted N_d (shown with blue and red histograms) and the FSSP measured N_d (the same black histogram in each panel). Predicted average N_d is noted for each case with $\langle N_d \rangle$ notation. The average in-cloud observed N_d is 223 cm^{-3} for all cases.

Initial analyses of the model runs indicate that case d shows the closest match to the average observed N_d of 223 cm^{-3} . However, as the CCN closure analysis indicated, κ of 1.0 does not realistically represent the measured aerosol population over a desert region. In the lower extreme of $\kappa = 0.1$ trial (case b), droplet over-predictions reach to 10% levels even though there is a better shape-wise comparison between the predicted and observed N_d histograms. Quantitatively, the maximum observed N_d is 322 cm^{-3} while the maximum predicted N_d is 455 cm^{-3} for case b. This difference could be explained by the fact that the parcel experiences higher SS under the low hygroscopic composition

assumption of the initialized aerosol as it is shown in Fig. 18, thus lower size particles growing as cloud droplets but at same time increasing the cloud droplet number concentration.

Even though $\kappa = 0.1$ and average w initialized runs do not differ in the predicted N_d , Fig. 20 shows the effect of κ assumption on the condensational particle growth history of 15 accumulation/coarse and 12 Aitken mode particles.

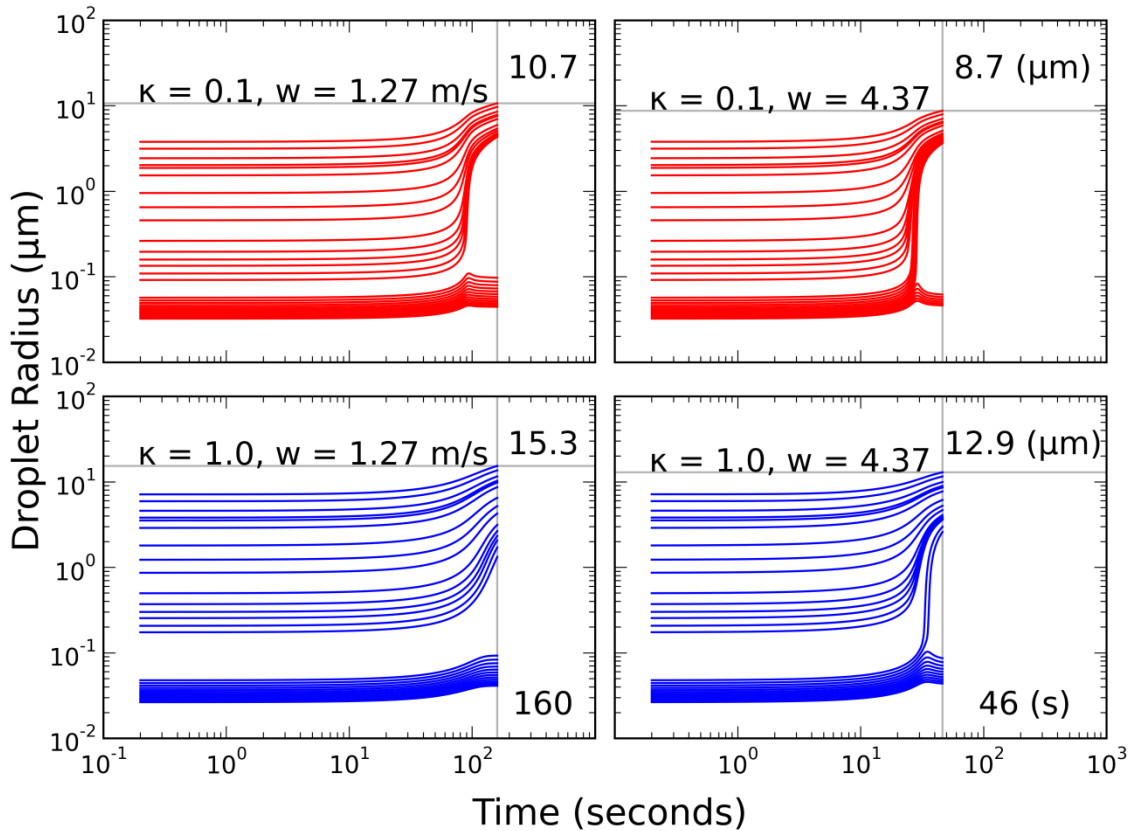


Figure 20: Growth history of four different setting initialized 15 accumulation/coarse and 12 Aitken mode aerosol. Note that $w=1.27 \text{ m s}^{-1}$ corresponds to the average updraft velocity in the cloud-base while 4.37 m s^{-1} is the maximum updraft observed in cloud-base. The cross-sections of the gray lines notes the maximum particle size reached within the parcel. The bottom two panels note the elapsed times until the parcels reach to the specified end-pressure point.

In the left two panels, for $\kappa = 1.0$ assumption case, particles can grow as big as $15.3 \mu\text{m}$ in radius compared to the $10.7 \mu\text{m}$ under $\kappa = 0.1$ assumption. When the tests were

repeated with the maximum w based parcel lifting assumption, although greater population of the aerosols are activated in the parcel, the maximum particle sizes can only reach to 75% of the average w based runs. The reason behind this difference is that in the higher w based run, the particles within the parcel can experience shorter amount of lifting (i.e., 46 seconds comparing to the 160 seconds), hence experience lesser condensational growth.

The comparison analysis is further extended with the inclusion of average w ($\langle w \rangle$) + one standard deviation of w (σ_w) and average PCASP aerosol ($\langle \text{PCASP} \rangle$) + one standard deviation of the PCASP aerosol (σ) based initialization settings to assess the sensitivities of the closure study. This makes it possible to compare parcel model predicted N_d results with the FSSP measured N_d for 12 different initializations. Table 9 provides each initialization setting and predicted and observed N_d in average \pm one standard deviation form and additionally noting the maximum observed and predicted cloud droplet concentration amounts.

Table 9: Cloud droplet number concentration comparison of 12 different way initialized parcel model runs. Note that the cloud-base measured average PCASP concentration ($\langle \text{PCASP} \rangle$) is 284 cm^{-3} with the standard deviation of 96 cm^{-3} .

Aerosol Init. Condition	Vertical Velocity (m s^{-1})		Observed N_d (cm^{-3})		Predicted N_d (cm^{-3})	
			$\langle N_d \rangle \pm \sigma$	$\text{max}(N_d)$	$\langle N_d \rangle \pm \sigma$	$\text{max}(N_d)$
$\kappa = 0.1$ $\langle \text{PCASP} \rangle$	$\langle w \rangle$	1.27	223 ± 66	322	188 ± 96	278
	$\langle w \rangle + \sigma_w$	2.35			145 ± 98	309
	w-PDF	[0.25..4.37]			245 ± 103	455
$\kappa = 1.0$ $\langle \text{PCASP} \rangle$	$\langle w \rangle$	1.27	223 ± 66	322	188 ± 96	278
	$\langle w \rangle + \sigma_w$	2.35			131 ± 88	278
	w-PDF	[0.25..4.37]			219 ± 96	338
$\kappa = 0.1$ $\langle \text{PCASP} \rangle + \sigma$	$\langle w \rangle$	1.27	223 ± 66	322	252 ± 129	372
	$\langle w \rangle + \sigma_w$	2.35			175 ± 118	372
	w-PDF	[0.25..4.37]			269 ± 114	372
$\kappa = 1.0$ $\langle \text{PCASP} \rangle + \sigma$	$\langle w \rangle$	1.27	223 ± 66	322	224 ± 115	331
	$\langle w \rangle + \sigma_w$	2.35			175 ± 118	372
	w-PDF	[0.25..4.37]			237 ± 114	372

The foremost consideration in the parcel initialization is the relative humidity

determination of the parcel condition. In all comparisons, the model runs were initiated with the maximum cloud-base observed RH condition, which was derived as 95% from the hygrometer measurements (the minimum cloud-base RH = 82%, while the average RH = 89%). Initialization of the parcel with the average 89% RH (for $\kappa = 0.1$ and 1.0 and using $\langle w \rangle$) does not yield any significant changes in the amount of N_d predictions, however the parcels can ascend nearly 400 m before the model execution stops. Greater ascent distance within the parcel leads to bigger particle sizes as a result of the condensational growth. In the $\kappa = 1.0$ simulation, accumulation/coarse mode particles can almost grow to 20 μm in radius size.

The second consideration is the construction of the Twomey fit using single point CCN measurement. Reliable construction of the $N = C s^k$ power-law based fit requires at least two or three distinct CCN spectra samples. Otherwise, the fitting routine (e.g., least-squares approach) fails to estimate the optimal fit parameters (i.e., C and k). We alleviated this situation by explicitly solving the fit equation for a single unknown C , using the k value estimated from the Apr02 ground-base CCN spectra fit. The rough approximated fit directly influences the determination of the Aitken mode section of the initialization CCN spectra. In Fig. 17, accumulation/coarse mode spectra better align with the Aitken mode for the $\kappa = 0.1$ assumption, but due to the restrictions in the current parcel model $\kappa = 1.0$ assumed aerosol modes cannot align in the spectral domain. Although, a quantitative assessment of the Aitken mode related initialization discrepancy cannot be made, the impact of this alignment should result in a negligible difference in the predicted N_d . This assumption is supported by the lower-right panel in the Fig. 20. Even under maximum w based parcel model execution, only two Aitken mode particles

can become activated and further be considered as predicted cloud droplet. In considering aerosol initialization, the average total PCASP aerosol concentration is 284 cm^{-3} with a standard deviation of 96 cm^{-3} . All the model runs listed in the Table 9 that were performed with the average PCASP plus one standard deviation produce higher N_d predictions than those using average PCASP aerosol concentrations.

The last but the most important consideration in the model initialization is the selection and application of the vertical velocity. Throughout the simulations parcels ascent with the a few different variations of cloud-base measured w . In the top panels of Fig. 16, histograms of cloud-base and in-cloud measured w are given to illustrate the differences in between these two measurements. Although cloud-base air flow follows a relatively well-defined path towards within the cloud, the two measurements show a quantitative difference in magnitudes. The maximum cloud-base w is a little over 4.5 m s^{-1} whereas the maximum in-cloud w is about 3.5 m s^{-1} . Simulations that are based on in-cloud w assumed parcel lifting show that predicted droplet number concentration increases with the reduced vertical velocity. It is important to note that PDF initialization of the vertical velocity in the model is treated with the same occurrence chance of all the binned w . That is to say, although the frequency of cloud base updrafts in the $0 - 0.5 \text{ m s}^{-1}$ bin is much greater than those in the $> 4 \text{ m s}^{-1}$ bin (see Fig. 16), these two bins are treated with equal chance of occurrence. A future update in the model initialization requires proper weighting of vertical velocities to better simulate the behavior of natural w distribution.

Conclusions

We conclude that desert region cumulus cloud measurements based CDNC closure

cannot be achieved using the average updraft assumption and the average PCASP aerosol concentration. The w-PDF initialized parcel simulations produced better agreement with the observed droplet concentration in terms of both the average amount and histogram shape comparisons. The average w based run only produced a well-agreeing result when the initialized aerosol was increased by about 34%. Even though the w-PDF based simulation predicts much closer average droplet concentration compared to the average w based parcel model simulations, usage of this value might be misleading for three important points: 1) clouds have much more complicated processes (e.g., entrainment, aerosol removal processes, non-constant updraft velocities) that are not easily implemented in the parcel model; 2) aerosol composition might show differences for the different particle size, which here is only addressed with a simplified single parameterization approach; and 3) measurement uncertainties exist in the actual observations (e.g., vertical velocity, aerosol and cloud droplet number concentration measurements). Establishing the high hygroscopicity assumption of super micron size aerosol, cloud droplets can grow as large as 15 μm radius size, possibly providing a promising outcome to artificially modify the precipitation forming process.

REFERENCES

- Andreae, M. O., and D. Rosenfeld, 2008: Aerosol-cloud-precipitation interactions. Part 1. The nature and sources of cloud-active aerosols. *Earth Science Reviews*, **89**, 13-41.
- Broekhuizen, K., R. Chang, W. Leitch, S. Li, and J. P. D. Abbatt, 2006: Closure between measured and modeled cloud condensation nuclei (CCN) using size-resolved aerosol compositions in downtown Toronto, *Atmos. Chem. Phys.*, **6**, 2513–2524.
- Covert, D. S., J. L. Gras, A. Wiedensohler, and F. Stratmann, 1998: Comparison of directly measured CCN with CCN modeled from the number-size distribution in the marine boundary layer during ACE 1 at Cape Grim, Tasmania, *J. Geophys. Res.*, **103**, 16 597–16 608.
- Delene, D. J., and G. Sever, 2009: Leak testing the DMT cloud condensation nuclei counter for deployment on pressurized aircraft, talk presented at the Droplet Measurement Technology Cloud Condensation Nuclei Workshop, December 10 in Boulder, Colorado.
- , M. R. Poellot, C. A. Grainger, J. S. Tilley, 2009: Kingdom of Saudi Arabia assessment of rainfall augmentation, 2009 spring field season final report. submitted to the Presidency of Meteorology and Environment, Kingdom of Saudi Arabia through Weather Modification Inc.
- , 2010: Aircraft Data Processing and Analysis Software Package, *Earth Science Informatics*, Accepted 23 July 2010, DOI: 10.1007/s12145-010-0061-4.
- DMT, 2007: Constant Pressure Inlet (CPI) Operator Manual, DOC-0125 Revision G.
- Dusek, U., G. P. Frank, L. Hildebrandt, J. Curtius, J. Schneider, S. Walter, D. Chand, F. Drewnick, S. Hings, D. Jung, S. Borrmann, and M. O. Andreae, 2006: Size matters more than chemistry for cloud nucleating ability of aerosol particles. *Science*, **312**, 1375–1378.
- Dye, J. E. and D. Baumgardner, 1984: Evaluation of the Forward Scattering Spectrometer Probe. Part I: Electronic and optical studies. *J. Atmos. Oceanic Technol.*, **1**, 329–344.

- Fountoukis, C., and A. Nenes, 2005: Continued development of a cloud droplet formation parameterization for global climate models, *J. Geophys. Res.*, **110**, D11212, doi:10.1029/2004JD005591.
- Fountoukis, C., A. Nenes, N. Meskhidze, R. Bahreini, W. C. Conant, H. Jonsson, S. Murphy, A. Sorooshian, V. Varutbangkul, F. Brechtel, R. C. Flagan, and J. H. Seinfeld, 2007: Aerosol – cloud drop concentration closure for clouds sampled during the International Consortium for Atmospheric Research on Transport and Transformation 2004 campaign, *J. Geophys. Res.*, **112**, D10S30.
- Garvey, D. M. and R. G. Pinnick, 1983: Response characteristics of the Particle Measuring Systems Active Scattering Aerosol Spectrometer Probe (ASASP-X). *Aeros. Sci. Tech.*, **2(4)**:477-488.
- Hobbs, P. V. (editor), 1993: *Aerosol Cloud Climate Interaction*. Academic Press, CA.
- IPCC, Solomon, S., Qin, D., Manning, M., Chen, Z., Marquis, M., Averyt, K., Tignor, M., and Miller, H. L., 2007: *Climate Change 2007: The Physical Science Basis, Contribution of Working Group I to the Fourth Assessment Report of the Intergovernmental Panel on Climate Change*, Cambridge and New York, Cambridge University Press, 996, 2007.
- Jacobson, M. Z., 2005: *Fundamentals of Atmospheric Modeling*. 2nd ed. Cambridge Univ. Press.
- Köhler, H., 1936: The nucleus in and the growth of hygroscopic droplets, *Trans Faraday Soc.*, **32**, 1152–1161.
- Levin, Z. and W. Cotton, (eds) 2008: *Aerosol Pollution Impact on Precipitation*. Springer.
- Liu, P. S. K., Leitch W. R., J. W. Strapp, and M. A. Wasey (1992), Response of particle measuring systems airborne ASASP and PCASP to NaCl and latex particles, *Aerosol Sci. Technol.*, **16**, 83-95.
- Lohmann, U., and Feichter, J., 2005: Global indirect aerosol effects: a review. *Atmos. Chem. Phys.* **5**, 715-737.
- Petters, M. D. and Kreidenweis, S. M., 2007: A single parameter representation of hygroscopic growth and cloud condensation nucleus activity, *Atmos. Chem. Phys.*, **7**, 1961-1971.
- Petters, M. D. and Kreidenweis, S. M., 2008: A single parameter representation of hygroscopic growth and cloud condensation nucleus activity: Part II: Including solubility, *Atmos Chem Phys.*, **8**, 6273-6279.

- Pruppacher, H. R., and J. D. Klett, 1997. *Microphysics of Clouds and Precipitation*. 2nd Edition. Kluwer, Dordrecht.
- Roberts, G. C., and A. Nenes, 2005: A continuous-flow streamwise thermal gradient CCN chamber for atmospheric measurements, *Aeros. Sci. Tech.*, **39**, 206–221.
- Rogers, R. R., and M. K. Yau, 1994: *A Short Course in Cloud Physics*. Pergamon Press.
- Rose, D., S. S. Gunthe, E. Mikhailov, G. P. Frank, U. Dusek, M. O. Andreae, U. Pöschl, 2008: Calibration and measurement uncertainties of a continuous-flow cloud condensation nuclei counter (DMT-CCNC): CCN activation of ammonium sulfate and sodium chloride aerosol particles in theory and experiment. *Atmospheric Chemistry and Physics*, **8**, 1153-1179.
- SciPy, E. Jones, T. Oliphant, P. Peterson, <http://www.scipy.org>
- Seinfeld, J. H., and S. N. Pandis, 2006: *Properties of Atmospheric Aerosol, in: Atmospheric Chemistry and Physics: From Air Pollution to Climate Change*. 2nd ed. Wiley-Interscience.
- Snider, J. R., S. Guibert, J.-L. Brenguier, and J.-P. Putaud, 2003: Aerosol activation in marine stratocumulus clouds: Part 2. Köhler and parcel theory closure studies, *J. Geophys. Res.*, **108(D15)**, 8629.
- Sotiropoulou, R.-E. P., J. Medina, and A. Nenes, 2006: CCN predictions: Is theory sufficient for assessments of the indirect effect?, *Geophys. Res. Lett.*, **33**, L05816, doi:10.1029/2005GL025148.
- Toon, O., J. Pollack, and B. Khare, 1976: The optical constants of several atmospheric aerosol species: ammonium sulfate, aluminum oxide, and sodium chloride, *J. Geophys. Res.*, **81(33)**, 5733-5748.
- TSI Inc., 2007: Model 3772 / 3371 Condensation Particle Counter Operation and Service Manual. P/N 1980529, Revision C.
- Twomey, S., 1959: The nuclei of natural cloud formation. Part II: The supersaturation in natural clouds and the variation of cloud droplet concentration. *Geophys. Pure Appl.*, **43**, 243–249.
- Zou, Y.-S., and N. Fukuta, 1999: The effect of diffusion kinetics on the supersaturation in clouds, *Atmos. Res.*, **52**, 115 – 141.